12-9-2022

The emerging value of the viroid model in understanding plant responses to foreign RNAs

Junfei Ma
Mississippi State University, 970173600@qq.com

The emerging value of the viroid model in understanding plant responses to foreign RNAs

By

Junfei Ma

Approved by:

Ying Wang (Major Professor)
Ling Li
Shien Lu
Bin Liu
Justin Thornton (Graduate Coordinator)
Rick Travis (Dean, College of Arts & Sciences)

A Dissertation
Submitted to the Faculty of
Mississippi State University
in Partial Fulfillment of the Requirements
for the Degree of Doctor of Philosophy
in Biological Sciences
in the Department of Biological Sciences

Mississippi State, Mississippi

December 2022

Name: Junfei Ma

Date of Degree: December 9, 2022

Institution: Mississippi State University

Major Field: Biological Sciences

Major Professor: Ying Wang

Title of Study: The emerging value of the viroid model in understanding plant responses to foreign RNAs

Pages in Study: 81

Candidate for Degree of Doctor of Philosophy

RNAs play essential roles in various biological processes. Mounting evidence has demonstrated that RNA subcellular localization and intercellular trafficking govern their functions in coordinating plant growth at the organismal level. Beyond that, plants constantly encounter foreign RNAs (*i.e.*, RNAs from pathogens including viruses and viroids). The subcellular localizations of RNAs are crucial for their function. While numerous types of RNAs (*i.e.*, mRNAs, small RNAs, rRNAs, tRNAs, and long noncoding RNAs) have been found to traffic in a non-cell-autonomous fashion within plants, the underlying regulatory mechanism remains unclear. Viroids are single-stranded circular noncoding RNAs, which entirely rely on their RNA motifs to exploit cellular machinery for organelle entry and exit, cell-to-cell movement through plasmodesmata, and systemic trafficking. Viroids represent an excellent model to dissect the role of RNA 3-dimensional (3D) structural motifs in regulating RNA movement. Using nuclear-replicating viroids as a model, we showed that cellular Importin alpha-4 is likely involved in viroid RNA nuclear import, empirically supporting the involvement of Importin-based cellular pathway in RNA nuclear import. We also confirmed the involvement of a cellular protein (Virp1) that binds both Importin alpha-4 and viroids. Moreover, a conserved C-

loop in nuclear-replicating viroids serves as a key signal for nuclear import. Disrupting C-loop impairs Virp1 binding, viroid nuclear accumulation and infectivity. Further, C-loop exists in a subviral satellite noncoding RNA that relies on Virp1 for nuclear import.

On the other hand, no viroid can systemically infect the model plant *Arabidopsis thaliana*, suggesting the existence of non-host resistance yet to be understood. Here, we attempted to test whether a gene involved in RNA silencing, RNA-dependent RNA polymerase 6 (RDR6), plays a role in non-host resistance in *Arabidopsis*. I will discuss the data below in detail.

DEDICATION

I dedicate this dissertation to my parents Dr. Zhonghua Zhang and Dr. Jianping Ma, and my friend Dr. Jie Hao for their support and encouragement.

ACKNOWLEDGEMENTS

I would like to thank my major advisor Dr. Ying Wang for encouraging me to presume many different projects in the past five years. He is skillful, enthusiastic, and lively. I am grateful to all my committee members Drs. Ling Li, Bin Liu, and Shien Lu for their scientific advice and insightful suggestions.

I would like to thank Dr. Shachinthaka Dissanayaka Mudiyanselage for his help in the laboratory and his contributions to my projects. Furthermore, I would like to acknowledge my lab mates and collaborators, including Lexie Thomas and Dr. Bin Liu for their support. I thank all the other students, staff, and faculty of the Department of Biological Sciences.

TABLE OF CONTENTS

LIST OF TABLES

LIST OF FIGURES

CHAPTER I

INTRODUCTION

This chapter is a slightly modified version of "Studies on viroid shed light on the role of RNA 3-dimensional structural motifs in RNA trafficking in plants" published in Frontiers in Plant Science [1] and has been reproduced here with the permission of the copyright holder. I have played a major role in developing the concepts in this chapter.

1.1 Studies on viroid shed light on the role of RNA 3-dimensional structural motifs in RNA trafficking in plants

Multicellular organisms evolve diverse mechanisms to integrate individual cells during development and in response to environmental cues. Cellular boundaries function in this integration through balancing cell autonomy and communication among cells [2]. In plants, neighboring cells are connected *via* plasmodesmata (PD), which are micro-channels crossing cell walls. The vascular system, including xylem and phloem, mediates the systemic transportation of molecules. The xylem system is mainly responsible for the transportation of water and minerals, while the phloem system transports photosynthates and macromolecules. Various proteins, RNAs, as well as viruses and viroids can be found in the translocation stream of phloem [3, 4].

Most cellular RNAs are transcribed in the nucleus, and then are either retained in the nucleus or transported to the cytoplasm for function. RNAs in the cytoplasm can participate in diverse biological activities and processes, or are transported to the nucleus performing various functions, or even traffic to neighboring cells to act as non-cell-autonomous regulators [5-9].

Non-cell autonomous RNAs widely exist in plants, and there are many types of those trafficking RNAs, including various small RNAs, mRNAs, tRNAs, rRNAs, and infectious RNAs from viruses and viroids [3, 4]. Some mobile RNAs will move short distance across several cells, while others move through various tissues to traffic systemically in plants [8, 10-13].

Non-cell autonomous RNAs serve as critical signals to regulate plant development and responses to biotic and abiotic challenges [3, 4, 14]. Using grafting experiments, some mRNAs are found to traffic long distance across the grafting junctions in regulating plant development, such as tuber formation in potato [15] and leaf morphogenesis in tomato [16, 17]. Related to plant physiology, a microRNA (miR399) has been found to move from shoot to root contributing to the maintenance of phosphate homeostasis in *Arabidopsis* [18, 19]. Numerous small RNAs, including miRNAs and short interfering RNAs (siRNAs), serve as long distance epigenetic signals coordinating gene expression and antiviral defense [20-22].

A key question remains regarding how RNA is selected for trafficking (including intracellular, intercellular, and systemic trafficking). A recent report showed that m^5C methylation is highly enriched in mobile mRNAs. Loss-of-methylation inhibits the non-cell-autonomous behavior of some mobile mRNAs [23]. This finding provides mechanistic insights into the selection specificity of mobile transcripts. However, it is unclear whether m^5C methylation ensures the accurate transportation of RNAs to their proper destiny within plants. RNAs by themselves also contain signals in regulating long distance RNA trafficking. For example, a *cis* element cloned from the 5' untranslated region (UTR) of a potexviral RNA mediates cell-to-cell movement of the fused GFP reporter RNA [24]. In addition, the UTRs of potato *BEL5* mRNA possess the regulatory elements for long distance trafficking [15]. The detailed molecular basis underlying these functional structures remains to be determined.

1.2 Viroids as a productive model to understand structure-based RNA trafficking

Viroids, single-stranded circular noncoding RNAs, harness cellular machinery to target specific organelles for replication, invade neighboring cells through plasmodesmata, and spread systemically *via* phloem [25]. Within phloem, viroids likely form an RNA-protein complex with phloem pectin PP2 for long distance translocation [26-28]. During systemic infection, viroid RNAs will move across various cellular boundaries [2, 14]. In a simplified view, viroids will traffic from epidermis, through palisade and spongy mesophyll and bundle sheath, to enter phloem. They will also traffic in a reverse direction in systemic leaves [29]. Viroids accumulate to high levels in plant cells, and it is easy to engineer various mutants for functional analyses [14]. There is no endogenous background signal interfering with analyses on viroid RNAs. Therefore, viroid infection provides a valuable experimental system to dissect the factors and regulatory mechanisms underlying RNA movement in plants.

Given that viroids do not encode any proteins, their RNA genomes must contain explicit information to guide cellular machinery for accurate localization and trafficking. Using potato spindle tuber viroid (PSTVd) as a model, specific RNA 3-dimensional (3D) motifs responsible for crossing multiple cellular boundaries have been identified, providing solid genetic evidence that those RNA motifs guide specific trafficking in plants [25, 30, 31]. It is noteworthy that the secondary structure of viroid RNAs are among the best-known structures thanks to the extensive chemical mapping analyses [32-36], which paves the way to further pinpoint to the functional structures of local RNA 3D motifs.

1.3 Essential role of non-Watson Crick base pairing in RNA loop motifs

RNA molecules form various helices and loops in their secondary structures. Helices are composed of contiguous Watson-Crick (WC) base pairs (*i.e.*, adenine [A]–uridine [U], guanine

[G]–cytosine [C], and GU base pairs). In contrast, loop regions are composed of diverse non-WC base pairs that are highly arranged [31]. Many loop motifs can be found at nonhomologous positions of diverse RNA species but largely keep the base pair geometries and interaction details, so they are also termed recurring loop motifs [37]. RNA 3D loop motifs provide recognition sites for specific RNA-protein, RNA-RNA, and RNA-ligand interactions. This is feasible thanks to the non-WC base pairs that widen the major groove of RNAs and expose distinct WC edges of four bases [31]. Each RNA base has three edges (*i.e.*, the WC, Hoogsteen, and Sugar edges) that can participate in interaction with other base edges to form non-WC base pairs in loop motifs (Figure 1.1).

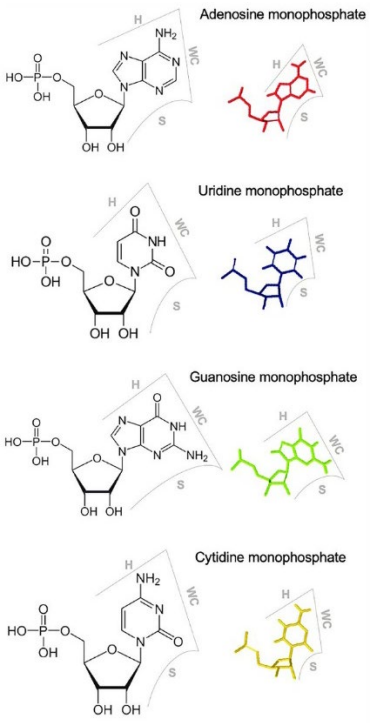

Figure 1.1 Three edges of RNA nucleotides.

WC, Watson-Crick edge; H, Hoogsteen edge; S, sugar edge.

1.4 A C-loop for RNA nuclear import

Viroids of the family *Pospiviroidae* all enter the nucleus for replication. How RNA nuclear import is regulated remains as an interesting question. Most RNAs are made in the nucleus, and the prevailing view is that those RNAs either traffic to the cytoplasm or remain in the nucleus for function. In recent years, more and more RNAs, besides viroids, have been found to enter the nucleus [5, 9, 38-42]. Using PSTVd as a model, data from one of my Ph.D. projects illustrate that viroids exploit cellular importin alpha-4 (IMPa-4) based pathway and a viroid-binding protein (Virp1) to achieve nuclear import [43].

Previous studies have mapped a region in viroid RNA genomes responsible for Virp1 binding, termed RY motif [44, 45]. However, the molecular basis of the RY motif for Virp1 recognition remains elusive. Recently, we carefully re-examine the RY motif in PSTVd and uncovered a C-loop structure within the region. C-loop is an asymmetric loop that has been found in many rRNAs, mammalian noncoding RNAs, and one bacterial mRNA [46-49]. C-loop has the following features: A) "C" is often the first base in the longer strand; B) two bases in the longer strand form non-WC base pairs with bases in the opposite strand (*cis*-WC-sugar and *trans*-WC-Hoogsteen base-pairings); C) two triads are formed through base-pairings from two strands; D) this motif is often found in hairpin stem-loop structure [47, 49]. PSTVd C-loop is composed of C189-A173 *cis*-WC-sugar base-pairing and A171-U187 *trans*-WC-Hoogsteen base-pairing (Figure 1.2), which is supported by chemical mapping data and functional mutagenesis analyses [43]. Our data showed that C-loop is pivotal for Virp1-binding, viroid nuclear accumulation, and infectivity. Interestingly, C-loop can be found in nearly all, except one, formal members of the family *Pospiviroidae* as well as a viral satellite RNA that relies on Virp1 for nuclear import [43].

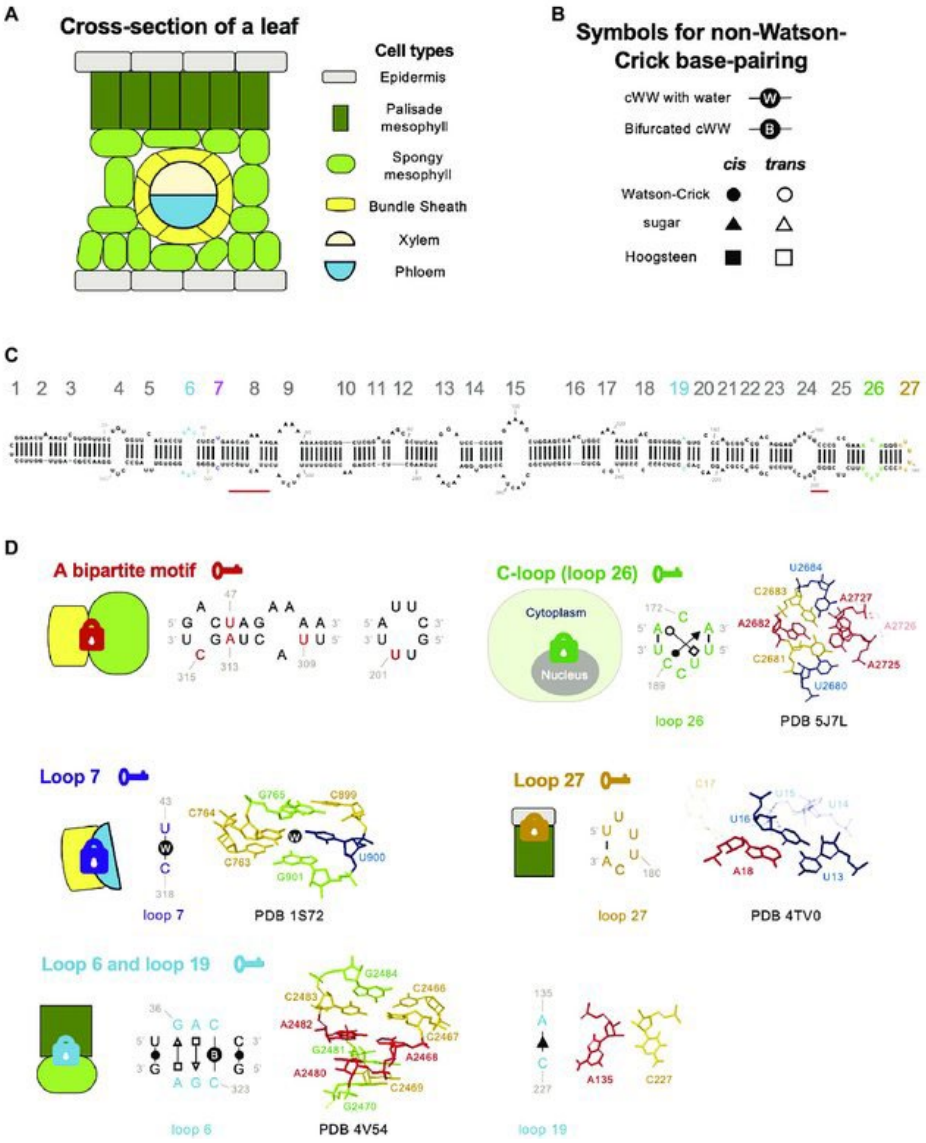

Figure 1.2 RNA 3D motif-mediated viroid RNA trafficking in plants.

(A) Cartoon illustration of the cross-section of plant leaves. (B) Symbols for annotating RNA nucleotide edges. cWW, *cis*-Watson Crick-Watson Crick base-pairing. (C) The secondary structure of the PSTVd ^{Int} genome, drawing by using RNA2Drawer [50]. Loops and bulges are numbered from left to right as 1 to 27. Key structural motifs illustrated in (D) are highlighted in colors (nucleotides and loop numbers). The nucleotides of the bipartite motif (position indicated by two red bars) are not color-highlighted in the secondary structure because this motif was only found in the PSTVd ^{NB} strain, whose secondary structure has not been confirmed by chemical probing. (D) Loop structures critical for regulating trafficking across cellular boundaries. Locks with different colors indicate distinct barriers that restrain the trafficking of RNAs without necessary RNA motifs ("keys"). The annotated base-pairings were validated by chemical mapping and functional mutagenesis. The C-loop structure model is based on regions 2,680-2,684 (5'-UCACU-3') and 2,725-2,727 (5'-AAA-3') of bacterial 23S rRNA (PDB 5J7L; [51]).

Figure 1.2 (continued)

The loop 7 structural model is based on regions 763-765 (5'-CCG-3') and 899-901 (5'-CUG-3') of Haloarcula marismortui 23S rRNA (PDB 1S72; [52]). The loop 27 model is based on the region 13-18 (5'-UUUUCA-3') of a Drosophila histone mRNA (PDB 4TV0; [53]). The loop 6 model is based on regions 2,466-2,470 (5'-CCACG-3') and 2,480-2,484 (5'-AGACG-3') of bacterial 23S rRNA (PDB 4V54; [54]). Note that C2483 and C2467 form a bifurcated cWW base-pairing. The illustration for loop 19 is extracted from the RNA Basepair Catalog. Nucleotides in transparent indicate that they are not involved in base interactions (e.g., A2726 in PDB 5J7L).

Therefore, C-loop is probably a widely used RNA motif for the nuclear import of subviral RNAs. Given that the nuclear import of RNAs is not limited to subviral agents, this finding will encourage new efforts to cast a wider net in search for more regulatory RNA motifs responsible for nuclear import.

1.5 A bipartite structure mediating the exit of bundle sheath

It is intuitive to reason that viroid RNAs contain the necessary information for cell-to-cell and even long-distance trafficking. Early work using PSTVd sequence in chimeric RNAs supports this hypothesis [55]. Analyses on PSTVd^{NT} and PSTVd^{NB} strains provided the first empirical evidence illustrating an RNA motif responsible for regulating trafficking across cellular boundaries [56]. PSTVd^{NT} harbors a spontaneous nucleotide substitution C259U in the tomato isolate PSTVd$^{KF440-2}$ that enables infection in tobacco (*Nicotiana tabacum*) [57]. PSTVd^{NB} accumulated five more spontaneous mutations (G210U, A309U, A47U/U313A, and U315C) during vegetative propagation through cuttings from PSTVd^{NT}-infected tobacco plants [56]. PSTVd^{NT} and PSTVd^{NB} bear similar replication efficiency in protoplasts but display different accumulation levels in systemic leaves. *In situ* hybridization analyses showed that PSTVd^{NB}, but not PSTVd^{NT}, can exit the bundle sheath to invade more cells in systemic leaves [56].

Mutational analyses found that four out of the five spontaneous mutations in PSTVd^{NB} are both required and sufficient to enable bundle sheath exit in tobacco. Interestingly, these substitutions are clustered in two discrete regions in the PSTVd genome forming a bipartite motif (Figure 1.2) [56]. The detailed structural basis of this bipartite motif remains elusive. It is noteworthy that this bipartite motif appears to be required for unidirectional bundle sheath exit only in tobacco but not in tomato or *Nicotiana benthamiana* (*N. benthamiana*), indicating that those RNA motifs can evolve very fast in nature and influence the host tropism of infectious RNAs.

1.6 An RNA motif for phloem loading

An early attempt to screen for PSTVd loss-of-function trafficking mutants identified two nucleotides (U43 and C318) that did not affect replication but abolished systemic trafficking [58]. Interestingly, U43 and C318 form a one base-pairing loop, loop 7 (Figure 1.2). Using *in situ* hybridization analyses found that loop "close" mutants (U43G or C318A) were present in epidermis, mesophyll, and bundle sheath cells but could not be loaded into phloem. It is unclear whether this regulation is unidirectional or bidirectional because transgenic expression of loop 7 mutants in companion cells all converted to wildtype sequences, rendering it difficult to access the regulation of trafficking direction.

Using the FR3D program to search for similar loop structures obtained by highest-resolution X-ray crystallography in the Protein Data Bank (PDB) revealed that U43 and C318 form a *cis*-WC-WC base pair with a water molecule insertion (Figure 1.2) [58]. All the mutants predicted to retain the structure for water insertion were able to traffic systemically in plants, whereas the mutants predicted to form canonical WC-WC base-pairing without water insertion failed to traffic out of inoculated leaves. The water molecule insertion widens the minor groove

and increases the angle subtended by the glycosidic bonds, presumably favoring protein binding [58]. Indeed, similar structures in rRNAs and siRNA duplexes are involved in protein binding [59, 60].

1.7 Genome-wide analyses uncovering multiple loops in PSTVd regulating systemic trafficking

The discovery of loop 7 and the bipartite motif inspired the idea that there exist elegant regulations at each cellular boundary regulating the exchange of cellular contents, including RNAs. Accordingly, multiple RNA motifs will work in concert to coordinate trafficking across those cellular boundaries. Therefore, genome-wide functional analyses of PSTVd loop motifs were performed to access the role of each loop motif in regulating replication and systemic trafficking [61]. By replacing all possible non-WC base-pairings in loop motifs with WC base-pairings, a series of mutants were generated to "close" every loop motif except loop 15 and loop 7 that have been previously annotated before this study. These loop mutants were tested for replication ability in protoplasts and systemic trafficking in *N. benthamiana* plants. A total of 11 loop mutants were found to impair systemic trafficking [61]. Some of the loops, such as loop 6, loop 19, and loop 27, were subsequently found to regulate the trafficking across distinct cellular boundaries (see below for details). It is noteworthy that this analysis may overlook some more complex structures, such as the aforementioned bipartite motif. In addition, loop 26 mutant did not show trafficking because it regulates nuclear import as aforementioned [43]. Nevertheless, this approach provides an overview of the genomic organization of viroids in controlling trafficking in *N. benthamiana*. Expanding this approach to other viroids, viruses, as well as diverse host-viroid combinations may achieve a much deeper understanding of structural motif-regulated RNA trafficking in plants.

1.8 A UNCG-like motif mediating unidirectional movement from epidermis to palisade mesophyll

Upon inoculation, viroid inoculum will initiate replication and then move through mesophyll layers to enter phloem. A recent study showed that the right terminal loop (loop 27) of PSTVd is critical for RNA moving from epidermis to palisade mesophyll [62]. Mutagenesis analyses showed that most mutants disrupting this loop led to failure in replication, except for the U178G/U179G mutation. The U178G/U179G mutant could spread within epidermis of inoculated leaves but was restrained from entering the adjacent palisade mesophyll layer as observed *via in situ* hybridization assay. Interestingly, needle punch delivery of this mutant into stems allowed mutant RNA to move across all cellular boundaries including from palisade mesophyll to epidermis in systemic leaves, indicating that this loop regulates unidirectional trafficking [62].

Using the JAR3D program [63], the terminal loop is predicted to be a UNCG-like motif (http://rna.bgsu.edu/rna3dhub/motif/view/HL_27353.2). The exact homolog loop can be found in the 3' UTR of a Drosophila histone mRNA, where the loop is involved in protein binding [64]. Within the loop region (nucleotides U177 to A182), U179 and C181 bulge outside of the motif. U180 stacks on the WC-WC pair (U177-A182) that closes the motif (Figure 1.2). It is believed that this loop does not contain stable non-WC base-pairings when the protein partner is absent [62].

1.9 Two RNA motifs for movement between palisade and spongy mesophyll

When a similar *in situ* hybridization analysis was performed using loop 6 mutants to determine the role of loop 6 in regulating viroid movements, those mutants, if replicable, were trapped in palisade mesophyll cells without entering spongy mesophyll [65]. A more recent work

on loop 19 mutants also revealed a similar pattern that loop 19 mutants accumulated in palisade mesophyll but could not enter spongy mesophyll [66]. It represents the first example where two RNA motifs regulate trafficking across the same cellular boundary. However, it cannot be ruled out that these two motifs form a larger bipartite organization to coordinate functions.

PSTVd loop 6 contains three non-WC base pairs: C323-C38 *cis*-WC-WC bifurcated pair, G324-A37 *trans*-Sugar-Hoogsteen (*t*SH) pair, and A325-G36 *trans*-Hoogsteen-Sugar (*t*HS) pair (Figure 1.2) [65]. The C323-C38 *cis*-WC-WC bifurcated pair is so rigid that it cannot be replaced by any other substitution. The *t*SH and *t*HS pairs can be substituted by some but not all isosteric base-pairings, implying the existence of other selection pressures [65]. Loop 6 is conserved in viroids belonging to the genus *Pospiviroid*. Similar loop motifs can also be found in some 16S rRNAs, 23S rRNAs, and a group I intron, where this structural motif serves as a binding site for protein partners [65]. Loop 19 is a one base-pairing loop [67]. This motif can emerge through spontaneous base substitutions in plants inoculated with loop-close mutants. Mutational analyses found that loop 19 is likely composed of a *cis* Sugar-Sugar base-pairing (Figure 1.2) [67].

1.10 Discussion

Emerging evidence supports the model that multiple structural motifs coordinate RNA subcellular localization and trafficking across different cellular boundaries within a plant. Those structural motifs act like “keys” to unlock restrictions at organellar gates as well as various cellular boundaries. A reasonable hypothesis is that those RNA 3D motifs are recognized by certain cellular proteins forming RNA-protein complexes, which will then be delivered to their destinations. In support of this model, the PSTVd C-loop serves a nuclear import signal recognized by cellular protein Virp1. The Virp1-PSTVd complex is then delivered into the

nucleus *via* the IMPa-4 based nuclear import pathway [43]. The detailed data on the nuclear import of PSTVd and its relatives are present in Chapters III and IV. In addition, recent evidence supports that an Exportin 5 ortholog (HASTY) participates in miRNA cell-to-cell and vascular movement in plants [68]. On the other hand, the molecular basis of those barriers at various cellular boundaries remains to be determined. It is intuitive to reason that PDs may adopt different selectivity when connect various types of cells. Diverse groups of proteins contribute to cargo targeting to PD and/or PD gating, including specific β-1,3-Glucanases for callose deposition and other PD-associated or mobile proteins [3, 69-72]. Those components may have different homologs or activities in distinct tissues, which can explain the need of multiple RNA motifs for crossing various cellular boundaries.

The complexity in organizing the required RNA motifs for RNA trafficking is intriguing. Some RNA motifs act in a species-specific manner while others work in concert to cross one specific cellular boundary, reflecting the sophisticated design in maintaining the autonomy of various tissues in different plants. To gain a deeper understanding of the barriers of cellular boundaries in different plants, analyzing the requirement of PSTVd trafficking motifs in different host-viroid combinations will be a straightforward approach to provide informative insights. Given the importance of RNA 3D motifs in host-viroid interactions, they certainly play a role in constraining viroid evolution and adaptation to new hosts [31]. On the other hand, emerging evidence (*e.g.*, bipartite as well as Loops 6 and 19) supports that viroid RNAs may undergo significant changes in overall structure to carry out functions. Currently, viroid RNA structures are mostly probed using *in vitro* assays. It will be beneficial to gain more insights into viroid structures at distinct subcellular and cellular compartments using *in vivo* probing methods,

particularly those that can achieve observation at the single molecular level to detect the transient structural changes [73-76].

It is desired that the knowledge gained from the viroid model can facilitate the understanding of cellular RNA trafficking. Increasing evidence supports that regulatory RNA structures can control endogenous RNA trafficking in plants, especially those tRNA-like structures (TLS) that have been identified in many endogenous mobile transcripts [77]. However, the detailed 3D base-pairing geometries, which confers the regulatory function in RNA trafficking in plants, have not been annotated for those regulatory structures. This is likely due to the technical limitations that hinders the discovery of such functional motifs. First, recurring RNA motifs may not exert the same function in different RNAs. For example, both PSTVd and 5S rRNA contain the Loop E motif [78]. However, a cellular protein, TFIIIA-9ZF, only binds the Loop E in 5S rRNA [79] but not the one in PSTVd [80]. Therefore, it is difficult to predict the function of recurring RNA motifs in distinct RNAs at this stage. Second, most cellular RNAs do not have well-annotated secondary structure, except for ribosomal RNAs, tRNAs, etc. The well-annotated secondary structure is a prerequisite for analyzing local 3D motifs. With the rapid development of novel probing methods for analyzing RNA structures at the transcriptome level [81-83], this limitation will soon be mitigated.

The discovery of m^5C methylation as a regulatory mark for mRNA translocation crossing graft junctions is a significant advancement in understanding the trafficking of endogenous RNAs [23]. However, the m^5C mark is enriched mostly four nucleotides downstream of the start codon in plant mRNAs [84] and promotes the efficiency of mRNA translation [85]. How the two biological processes (*i.e.*, translation and selection for trafficking) are balanced remains to be elucidated. Viroid RNAs do not possess m^5C modification [86], demonstrating that more than

one mechanism exists for selecting mobile RNAs. How these mechanisms are coordinated for accurate delivery of RNAs to destiny remains unexplored, which deserves future investigations.

CHAPTER II

RNA-DEPENDENT RNA POLYMERASE 6 MIGHT CONFER *ARABIDOPSIS* NON-HOST RESISTANCE AGAINST POTATO SPINDLE TUBER VIROID

2.1 Introduction

Plants are constantly challenged by various pathogens in the environment, including bacteria, fungi, nematodes, and even parasitic plants. Some challenges are repelled by plants, resulting in failure of colonization or propagation of a given pathogen species in these so-called non-host plants. To protect them from invasive pathogens, plants generally deploy a two-layer defense mechanism against various pathogens, namely pathogen-associated molecular patterns (PAMPs)-triggered immunity (PTI) and effector-triggered immunity (ETI) [87].

Viroids are single-stranded circular noncoding RNAs and known as the smallest nucleic acid-based pathogens. To date, nearly forty different viroids infecting a broad spectrum of crops have been identified [88]. Interestingly, none of the known viroids can systematically infect *Arabidopsis thaliana*, despite that viroids can replicate in *Arabidopsis* using the transgenic approach or protoplast assays [89]. Thus, *Arabidopsis* is considered to possess non-host resistance against all known viroids. Nevertheless, no resistance gene has been reported against any viroid in either host or non-host plants.

Current knowledge describes that RNA silencing plays a major role in defending viroid infection in host plants [90]. In plants, dicer-like proteins (DCLs), RNA-dependent RNA polymerases (RDRs) and Argonaute (AGOs) proteins are major players in RNA silencing.

Briefly, DCLs dice various double-stranded RNAs (dsRNAs) to generate small RNAs (sRNAs) about 20-24 nt in length, which are then loaded into AGOs to regulate the downstream targets. RDRs are involved in amplifying certain RNA templates to dsRNAs for dicing. DCL2 and DCL3 synergistically suppress PSTVd infection, whereas DCL4 somehow positively regulates PSTVd replication in *Nicotiana benthamiana* [91, 92]. Viroid-derived sRNAs can be loaded into AGOs to perform function [93, 94]. RDRs share the C-terminal DLDGD amino acid motif and have orthologs in many plant species[95]. In post transcription gene silencing (PTGS), virus RNAs amplified by RDR6 are processed into 21 nt siRNA by DCL4 and subsequently load into AGOs [96-98]. In addition, RDR6, a critical player in the RNA silencing pathway, prevents potato spindle tuber viroid (PSTVd) from invading shoot apical meristem (SAM) in host plants (*i.e.*, *N. benthamiana* and tomato) [99, 100]. However, whether RNA silencing contributes to constraining viroid host tropism remains elusive.

2.2 Materials and methods

2.2.1 Plant growth

A. thaliana plants were grown in a growth chamber at 22 °C and with a 10/14 h light/dark cycle. Mutant lines (Table A.2) were obtained from ABRC (Ohio State University, Columbus, OH). All mutants were verified using genotyping. Genotyping primers were listed in Table A.3. *Arabidopsis* plants with 12 true leaves were inoculated with mixed *in vitro* transcripts of $PSTVd^{Nb}$ and $PSTVd^{RG-1}$.

2.2.2 Cloning

All primers were listed in Table A.3. All the clones and constructs were sequenced at the core genomic facility at Arizona State University.

2.2.2.1 Generating riboprobes

pInt(-) for PSTVd has been described previously [101]. cDNAs of ASBVd, ASSVd, HLVd, CBCVd were commercially synthesized (Genscript, Piscataway, NJ). The cDNA products were treated with *Bsm*BI- (AFCVd) or *Bsa*I- (ASSVd, HLVd, CBCVd) based golden gate assembly kits (New England Biolabs, Ipswich, MA) and ligated to *Nco*I and *Not*I restricted pGEM-T vector (Promega, Madison, WI) for the corresponding monomer constructs. pASBVd-monomer was based on pCR4 vector (Thermo Fisher Scientific, Waltham, MA) *via* insertion of ASBVd cDNA cloned from pASBVd-dimer (inherited from the late professor Dr. Biao Ding at Ohio State University) *via* ASBVd-f and ASBVd-r primers. pHSVd-monomer was based on pGEM-T vector *via* insertion of HSVd cDNA cloned from HSVd-RZ plasmid (a gift from Dr. Robert Owens at USDA-ARS) *via* HSVd-f and HSVd-r primers.

For PSTVd, pInt(-) was linearized by *Spe*I (New England Biolabs) as the template and T7 MAXIscript kit (Thermo Fisher Scientific) was used to generate probe. For AFCVd, ASSVd, HLVd, and CBCVd, the corresponding plasmids were restricted by *Apa*I (New England Biolabs) as templates and SP6 MAXIscript kit (Thermo Fisher Scientific) was used to generate probes. For ASBVd, the pASBVd-monomer was linearized by *Not*I (New England Biolabs) as the template and T3 MAXIscript kit (Thermo Fisher Scientific) was used to generate probe. For HSVd, the pHSVd-Monomer was linearized by *Nco*I (New England Biolabs) as the template and SP6 MAXIscript kit was used to generate probe.

2.2.2.2 Generating inoculum RNA

pRZ:PSTVd^{NB} and pRZ:PSTVd^{RG-1} constructs have been described previously [87]. For AFCVd, ASSVd, HLVd, and CBCVd, their dimer constructs were cloned from the aforementioned corresponding monomer constructs following a published protocol [88].

pASBVd-dimer harbors two tandemly arranged ASBVd cDNA (isolate Uruapan-1) in the 154-153 orientation. pT3:HSVdRZ (Tu HSVd2-7 in the 83-82 orientation) used pGEM-T vector with insertion cloned from HSVd-RZ *via* T3-HSVd-f and RZ-r primers.

pRZ:PSTVd^{NB} and pRZ:PSTVd^{RG-1} were linearized by *Hin*dIII (New England Biolabs) followed by *in vitro* transcription using T7 MEGAscript kit (Thermo Fisher Scientific). The constructs for AFCVd, ASSVd, HLVd, and CBCVd were all restricted by *Nde*I (New England Biolabs) followed by *in vitro* transcription using T7 MEGAscript kit. pASBVd-dimer was restricted by *Xba*I (New England Biolabs) followed by *in vitro* transcription using T3 MEGAscript kit (Thermo Fisher Scientific). pT3:HSVdRZ was linearized by *Hin*dIII followed by *in vitro* transcription using T3 MEGAscript kit. All RNA *in vitro* transcripts were purified using the MEGAclear kit (Thermo Fisher Scientific).

2.2.3 RNA extraction and gel blots

RNAs were isolated using RNAzolRT (Molecular Research Center, Cincinnati, OH) and the purified RNAs were then subjected to RNA gel blots or Reverse transcription-PCR. Total RNAs were subjected to 5% (w/v) polyacrylamide/8 M urea gel for 1 hr at 200 V. Then RNA was transferred to Hybond-XL nylon membrane (GE Healthcare Lifesciences) using the Trans-Blot SD semi-dry transfer cell (Bio-Rad Laboratories) followed by UV cross-linking. Membranes were blocked by ULTRAhyb ultrasensitive hybridization buffer (Thermo Fisher Scientific) followed by overnight hybridization with (DIG)-labeled riboprobes at 65 °C (except 55 °C for the HSVd). Following the instructions of the DIG northern starter kit (Millipore Sigma), membranes were washed and incubated with antibody against DIG labeling. Transcripts were identified using the Immuno-Star AP chemiluminescence kit (Bio-Rad Laboratories). Signals were obtained using ChemiDoc (Bio-Rad Laboratories).

To verify PSTVd progeny sequence, about 100 ng total RNA from each infected plant were pooled and subject to reverse transcription using SuperScript III enzyme kit (Thermo Fisher Scientific) and primer 94r. The cDNA was PCR amplified (95f and 94r) and ligated to pGEM-T.

2.3 Results

To understand whether RNA silencing machinery confers *Arabidopsis* non-host resistance against viroids, we chose eight representative mutants (*dcl2-1*, *dcl4-2t*, *dcl2-1*/*dcl3-1*, *dcl3-1*/*dcl4-2t*, *rdr2-2*, *rdr6-15*, *ago2-1*, *sgs3-14*) involved in the RNA silencing pathway (Figure 2.1). All the mutants were well characterized and widely used. SGS3, RDR6, and DCL4 function in the same axis in generating phased secondary siRNAs [102], whereas RDR2 is a key component in 24 nt siRNA metabolism and epigenetic regulations [103]. Since AGO2 loss-of-function enables potato virus X to systemically infect *Arabidopsis* [104], this mutant is also included.

Given our failed experience in infecting wild type *A. thaliana* with PSTVd Intermediate (Int) strain (data not shown), we used a mixture of highly infectious NB and RG-1 strains of PSTVd as inoculum to increase the chance of success. As shown in Figure 2.1, PSTVd cannot systemically infect any of those mutants except rdr6. Remarkably, that PSTVd failed to invade DCL mutants (*i.e.*, *dcl2*, *dcl4*, *dcl2*/*dcl3*, *dcl3*/*dcl4*), providing empirical evidence that DCL genes are likely insufficient in defending viroid in *Arabidopsis*. Despite that PSTVd-infected *rdr6* plants did not exhibit any symptom, RDR6 may plays a major non-host resistance role against PSTVd in *Arabidopsis*. Unfortunately, this experiment cannot be well repeated after the first trial.

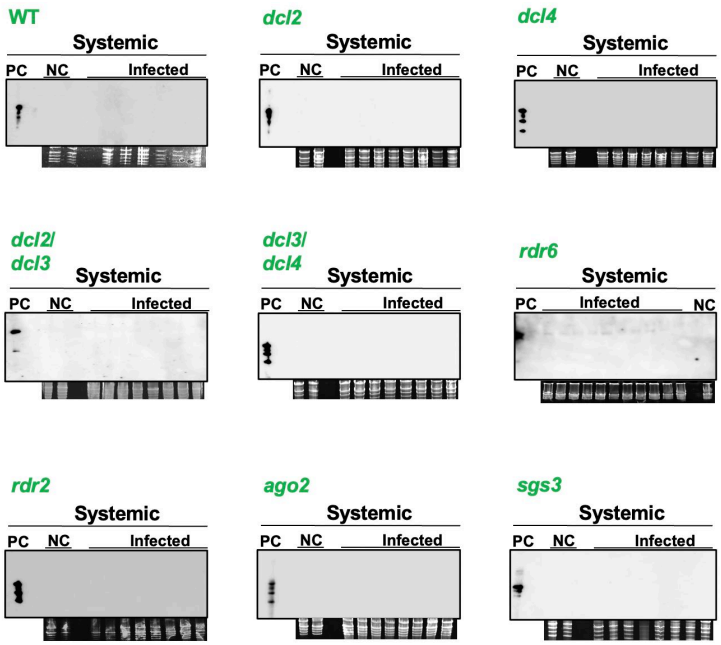

Figure 2.1 RNA gel blots detecting PSTVd infectivity in various *Arabidopsis* mutant.

Six to 8 plants of each mutant were used for this assay. RNAs from systemic leaves were subjected to RNA gel blots 21 days post infection. Ethidium bromide staining of ribosomal RNAs served as loading control. PC, *in vitro* transcripts as positive controls. NC, non-infected plants as negative controls.

Nevertheless, we could detect multiple PSTVd variants that arose in the systemic leaves of *Arabidopsis rdr6* plants in the successful replicate (Table A.1). Those sequenced PSTVd progeny in systemic leaves further corroborated the systemic trafficking of PSTVd in *rdr6* plants. We observed that multiple PSTVd variants arose in the systemic leaves (Table A.1), which reflects their adaptation to an arranged host. The NB strain was detectable in the systemic leaves, inferring its capacity in systemic infection. Interestingly, the intact RG-1 sequence was absent from the systemic leaves. Instead, there was one RG-1 sequence with an additional C230U mutation present among 16 clones, implying that RG-1 is unlikely infectious for *Arabidopsis*. Notably, the NT strain emerged during this adaptation, echoing a previous observation in which the NB strain emerged when infecting tobacco with the NT strain [105]. Of

note, the Intermediate (Int) strain, with a U259C conversion in NT sequence, became dominant in systemic leaves. Three out of 16 sequences were WT Int sequences, while another seven out 16 sequences accumulated additional mutations based on the Int sequence. Therefore, the 259 position of the PSTVd genome appears to be critical for host adaptation in *Arabidopsis*.

We employed six other viroids for the same infection assay, including avocado sunblotch viroid (ASBVd) in the family *Avsunviroidae* as well as hop stunt viroid (HSVd), apple fruit crinkle viroid (AFCVd), apple scar skin viroid (ASSVd), citrus bark cracking viroid (CBCVd), and hop latent viroid (HLVd) in the family *Pospiviroidae*. Members of the *Avsunviroidae* replicate in chloroplasts and are often termed chloroplastic viroids. In contrast, members of the *Pospiviroidae* replicate in the nucleus, so they are termed nuclear-replicating viroids. Interestingly, none of these tested viroids could establish systemic infection, despite that their inocula were stable in the local leaves (Figure 2.2).

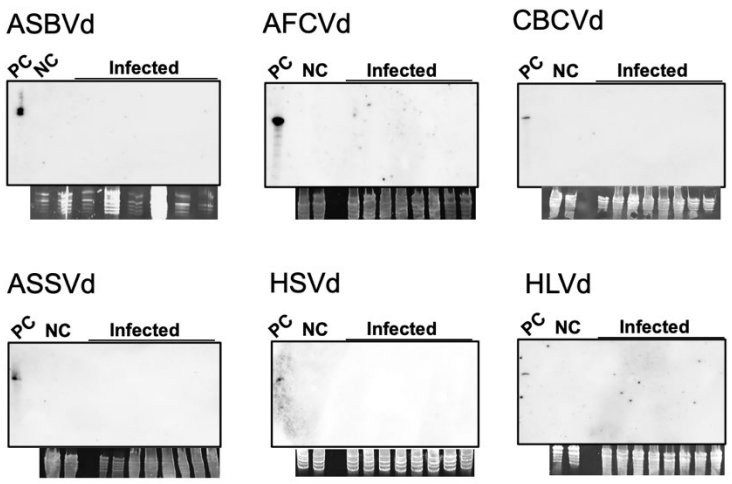

Figure 2.2 RNA gel blots detecting the infectivity of six viroids in *rdr6* plants.

Eight plants were used for each viroid. RNAs from systemic leaves were subjected to RNA gel blots 21 days post infection. Ethidium bromide staining of ribosomal RNAs served as loading control. PC, *in vitro* transcripts as positive controls. NC, non-infected plants as negative controls.

2.4 Discussion

Our results suggest *Arabidopsis* RDR6 as a potential non-host resistance gene against a viroid (*i.e*., PSTVd), which may provide mechanistic insights into non-host resistance against viroids. It is intriguing that certain player(s) in the RNA silencing machinery, rather than all the components has a potential to contribute to the non-host resistance and the host tropism. Unfortunately, we cannot repeat this experiment after the first success. It may be attributed to the dynamic gene expressions of plants at different physiological or developmental stages. Due to the poor reproducibility, we cannot make a strong conclusion at this stage.

Nevertheless, it becomes clear that plant defense against viroid infection relies on both RNA silencing and innate immunity based on a series of recent studies [106, 107]. Viroid infection generates small RNAs (sRNAs) ranging from 20–24 nt in size. These viroid-derived sRNAs (vd-sRNAs) likely play an inhibitory role in viroid replication. Viroid infection also triggers host immune responses that reprogram host gene expression to activate ROS signaling, cell wall fortification, and hormonal pathways related to defense. In general, the activation of immune responses often has impacts on plant signaling and metabolism that lead to cytopathic effects and alterations in morphology.

RNA-dependent RNA polymerase 6 (RDR6), a critical player in the RNA silencing pathway, plays a role in preventing PSTVd from invading shoot apical meristem in host plants (*i.e*., *N. benthamiana* and tomato) [99, 100]. Importantly, RDR6 also modulates HSVd-triggered pathogenicity in plants [108]. The detailed mechanism underlying the role of RDR6 in controlling PSTVd tissue tropism and pathogenicity remains to be determined. A recent report also shows that perturbing the expression of RDR1 affects PSTVd infectivity [109]. However, RDR1 expression remains unchanged in PSTVd- and CEVd-infected plants based on reported

RNA-Seq data [110, 111], rendering it questionable whether RDR1 is a *bona fide* defense gene against viroid.

CHAPTER III

A NUCLEAR IMPORT PATHWAY EXPLOITED BY PATHOGENIC NONCODING RNAs

This chapter is a slightly modified version of "A nuclear import pathway exploited by pathogenic noncoding RNAs" published in the Plant Cell [43] and has been reproduced here with the permission of the copyright holder.

3.1 Introduction

Most cellular RNAs are produced through transcription in the nucleus of eukaryotic cells and the prevailing view is that those RNAs either stay in the nucleus or move to the cytoplasm for function. Interestingly, emerging evidence showed that cellular RNAs (*i.e.*, small RNAs, tRNAs, and rRNAs), as well as viral RNAs, can traffic in the reverse direction from the cytoplasm to the nucleus. For instance, plant 24-nt heterochromatic small interfering RNAs (hc-siRNAs) are exported to the cytoplasm for Argonaute 4 loading before being redirected into the nucleus of the same cell or even neighboring cells for RNA-directed DNA methylation [5, 9]. In *Xenopus* oocytes, 5S rRNA relies on ribosomal protein L5 for nuclear import [38]. In another example, satellite RNA of Q-strain cucumber mosaic virus (Q-satRNA) relies on a bromodomain-containing cellular protein (Virp1) for entering the nucleus [42]. In contrast to the well-studied RNA nuclear export processes, the RNA nuclear import machinery and mechanism remain obscure, particularly regarding the molecular basis underlying the specific selection of RNAs for nuclear import.

To cross the double-membrane nuclear envelope, biomolecules need to traffic through the highly organized nuclear pore complexes (NPCs) in eukaryotic cells [112]. NPCs are conserved in eukaryotic organisms with some variations [113, 114]. Except for some free-diffusing small molecules below 40– 60kDa, most biomolecules rely on nuclear transport receptors (NTRs) to traffic through NPCs [112, 115-117]. Importin alpha subunits (IMPas) constitute a group of adapter proteins linking specific cargos to NTRs for crossing NPCs [112]. In *Arabidopsis thaliana*, nine IMPas play distinct yet partially redundant roles [112, 118]. Whether any IMPa is involved in RNA nuclear import remains to be determined.

Viroids are single-stranded circular noncoding RNAs that infect plants [88]. Due to their noncoding nature, viroids must utilize RNA structures to exploit cellular factors and complete their infection cycles. RNA secondary structures are primarily composed of helices and loops. RNA loops often form 3-dimensional (3D) structural motifs that contain highly arrayed non-Watson Crick-Watson Crick (non-WC-WC) base pairings and other base-specific interactions, including base stacking and base-backbone interactions [1, 31]. Each RNA base can use its three edges (*i.e.*, WC, Hoogsteen, and sugar edge) to form non-WC base-pairing geometries within a structural motif [1, 31]. Those non-WC base-pairings have been well documented in a large amount of atomic-resolution crystallography and NMR spectroscopy data (deposited in Protein Data Bank; https://www.rcsb.org). Several homology-based programs have been developed facilitating search for possible base-pairing geometry of a motif of interest [63, 119]. The RNA Basepair Catalog summarizes all possible non-WC base-pairings and their similarities from the deposited structural data [120], providing a valuable resource for analyzing non-WC base-pairings and for predicting functional substitutions [31]. Such an approach, in combination with

functional mutagenesis, has been successfully applied to analyze the structure-function relationships of multiple viroid motifs [58, 62, 65, 67, 121].

Viroid RNA secondary structures have been well annotated *via* various chemical mapping assays [32-35], providing a solid foundation to annotate base interaction geometries within loop motifs. A genome-wide analysis of potato spindle tuber viroid (PSTVd) RNA motifs has identified 11 out of 27 loop motifs responsible for systemic infection [61]. Some of those loop motifs regulate RNA trafficking across certain cellular boundaries, and their 3D structures have been successfully annotated using a combination of program prediction and functional mutagenesis [58, 62, 65, 67]. However, whether any RNA motif regulates viroid subcellular localization and organelle targeting remains unknown. Viroids of the family *Pospiviroidae* all replicate in the nucleus, and their nuclear import process is highly regulated [122, 123]. Hence, their noncoding RNA genomes likely contain the necessary information in certain forms (*e.g.*, an RNA 3D motif) to guide nuclear import. The cellular factor(s) for viroid nuclear import remains elusive as well. One viroid binding protein, Virp1, has been implied to accelerate the import of citrus exocortis viroid (CEVd), a relative of PSTVd within the same genus, to nuclei of onion (*Allium cepa*) cell strips [123]. Nevertheless, whether and how Virp1 regulates viroid nuclear import await to be clarified.

To gain a better understanding of RNA nuclear import, we identified *Arabidopsis* IMPORTIN ALPHA-4 (IMPa-4) as a cellular factor that can specifically enrich PSTVd through immunoprecipitation. Sl *IMPa-4*, the *IMPa-4* ortholog in tomato (*Solanum lycopersicum*), a host plant of PSTVd, is critical for infection. We also demonstrated the interaction between IMPa-4 and Virp1, which likely regulates Virp1 nuclear import. Moreover, we observed that Virp1 recognizes a specific RNA 3D motif, C-loop. C-loop can be found in PSTVd and hop stunt

viroid (HSVd) that belong to distinct genera. Mutational analyses showed that viroid C-loop is critical for Virp1 binding, viroid nuclear accumulation and infectivity. Notably, C-loop can be found in nearly all the nuclear-replicating viroids and also in the Q-satRNA that relies on Virp1 for nuclear import. Therefore, this work provides new insights into the biology of subviral RNAs. In addition, our data unravel a cellular pathway for RNA nuclear import and the molecular basis of a nuclear import signal in RNAs, which illustrates a nuclear import pathway for viral RNAs, and potentially cellular RNAs as well.

3.2 Materials and methods

3.2.1 Plant growth

We grew *Arabidopsis* plants in a growth chamber with a setting of 22°C and a 10/14 h light/dark cycle. We grew *N. benthamiana* and tomato (*S. lycopersicum*) plants in a growth chamber with a setting of 25°C and a 14/10 h light/dark cycle. Miracle-Gro all-purpose garden soil from local Lowe's store was used for plant growth. *N. benthamiana* and tomato seedlings at the four-leaf stage were inoculated with water or water containing 150 ng of *in vitro*-transcribed viroid RNAs. The viroid infection was analyzed by RNA gel blots using systemic leaves 3-week postinoculation. Agroinfiltration was performed following our established protocol [80].

3.2.2 DNA clones

cDNAs of some *Arabidopsis* Importin alpha subunits in pC-TAPa or Lic6 vectors were purchased from ABRC (Ohio State University, Columbus, OH): IMPa-1 (DKLAT3G06720), IMPa-2 (DKLAT4G16143), IMPa-3 (DKLAT4G02150), IMPa-4 (DKLAT1G09270), IMPa-5 (DKLAT5G49310.1) and IMPa-6 (DKLAT1G02690). IMPa-7 cDNA in pDONR221 vector (DQ446636) was purchased from ABRC and recombinated into pC-TAPa vector (ABRC) *via*

LR clonase (Thermo Fisher Scientific, Waltham, MA). IMPa-8 and IMPa-9 were amplified using gene-specific primers (Table A.5) and cloned into pCR8 (Thermo Fisher Scientific), which were then recombinated into pC-TAPa *via* LR clonase. It is noteworthy that the TAP tag in pC-TAPa contains 9X c-Myc tag, a His6 tag, and two IgG binding domains [124]. For BiFC, IMPa-1 and IMPa-4 cDNAs in entry vectors were recombinated into CD3-1651 (ABRC) using LR clonase.

To generate the pTRV2^{IMPa-4} clone, two specific primers (Table A.5) for *N. benthamiana* IMPa-4 fragment were used for genomic PCR and followed by digestion with *Bam*HI and *Xho*I (New England Biolabs, Ipswich, MA). The pTRV2^{vector} (CD3-1040) was obtained from ABRC. After linearization by *Bam*HI and *Xho*I, pTRV2^{vector} was used for ligation with the digested NbIMPa-4 fragments. Since we cannot reach 100% PSTVd infection in *N. benthamiana*, we then decided to use tomato for the VIGS assay. Based on the high sequence homology of IMPa-4 in tomato and *N. benthamiana*, we used the same pTRV2^{IMPa-4} clone for infiltration of tomato. Based on the BLAST search using Sol genomics database (https://solgenomics.net), our cloned fragment specifically targets IMPa-4 homologs in tomato and *N. benthamiana*. pTRV2^{GFP} (CD3-1044) is obtained from ABRC. pTRV2 variants in agrobacterium GV3101 were mixed with Agrobacterium harboring pTRV1 (ABRC) for VIGS infiltration into the first pair of true leaves of tomato seedlings, while cotyledons were used for inoculation with PSTVd RNA transcripts. Plants were subjected to RNA gel blot to analyze PSTVd and TRV titers, as well as the expression levels of IMPa-4 and Histone H2A (see Table A.5 for primer details). The TRV probe was described previously [125].

Virp1 and LHP1 from *Arabidopsis* were cloned *via* RT-PCT using gene-specific primers (Table A.5). The cloned cDNAs were inserted into pENTR vector (Thermo Fisher Scientific) and then recombinated into CD3-1637 (ABRC) or pMDC7 vector (modified to include a N-

FLAG tag; inherited from Biao Ding at Ohio State University) for agroinfiltration, pDEST15 vector (Thermo Fisher Scientific) for bacterial expression or CD3-1648 (ABRC) for BiFC, *via* LR clonase. Construct for expressing free GST in bacteria was a gift from Svetlana Folimonova at University of Florida.

The cDNAs of WT and mutant Q-satRNAs were commercially synthesized (Genscript, Piscataway, NJ). The cDNAs were amplified (see Table A.5 for primer sequences) and ligated into pGEM-T vector (Promega, Madison, WI). To generate RNA substrates for EMSA, *Spe*I (New England Biolabs) linearized plasmids (pGEMT-Q-satRNA^{WT} and pGEMT-Q-satRNA^{mu}) were subject to *in vitro* transcription using T7 MEGAscript kit (Thermo Fisher Scientific).

To generate RNA inocula, pRZ:Int construct [126] was by *Hin*dIII (New England Biolabs) followed by *in vitro* transcription using T7 MEGAscript kit. pT3:HSVd^{RZ} (Tu HSVd2-7 in the 83-82 orientation) used pGEM-T vector with the insertion cloned from HSVd-RZ (a gift from Dr. Robert Owens at USDA-ARS) *via* T3-HSVd-f and RZ-r primers (Table A.5). pT3:HSVd^{RZ} was linearized by *Hin*dIII followed by *in vitro* transcription using T3 MEGAscript kit (Thermo Fisher Scientific). All RNA *in vitro* transcripts were purified using the MEGAclear kit (Thermo Fisher Scientific).

To generate riboprobes, pInt(-) [127] was linearized by *Spe*I (New England Biolabs) as the template and T7 MAXIscript kit (Thermo Fisher Scientific) was used to generate probe. pHSVd-monomer was based on pGEM-T vector (Promega) *via* insertion of HSVd cDNA cloned from HSVd-RZ plasmid *via* HSVd-f and HSVd-r primers (Table A.5). The pHSVd-Monomer was linearized by *Nco*I (New England Biolabs) as the template and SP6 MAXIscript kit (Thermo Fisher Scientific) was used to generate probe.

To generate WT, A261C, and C-loop mutant constructs for agroinfiltration, the

corresponding pRZ:Int plasmids harboring the correct PSTVd cDNAs served as templates for PCR (using RZ-f and RZ-r primers; see Table A.5 for primer sequences). The PCR products were inserted into pENTR-D-TOPO vector (Thermo Fisher Scientific). The series of pENTR-RZ:Int plasmids were recombinated into CD3-1656 (ABRC) *via* LR clonase. The CD3-1656-RZ:Int plasmid series were transformed into Agrobacterium strain GV3101 for agroinfiltration.

All the constructs have been verified using Sanger sequencing.

3.2.3 RNA immunoprecipitation

RNA-immunoprecipitation (RIP) was performed according to a previously described protocol [80] with minor modifications. Briefly, PSTVd-infected *N. benthamiana* leaves were harvest 3 days post agroinfiltration of Importin alpha cDNAs. The cell lysates were incubated with magnetic mouse IgG beads (catalog #5873; Cell Signaling, Danvers, MA) for 2 h at 4°C. The input lysate and purified fractions were subject to immunoblotting and RT-PCR (after RNA purification). The primers for detecting PSTVd and Histone 2A mRNA were listed in Table A.5. RIP has been repeated at least twice for each IMPa gene. For each biological replicate, mixed leaf tissues from three or more plants were used for each treatment.

3.2.4 Co-Immunoprecipitation

Co-immunoprecipitation was following a recent report [128] with minor modifications. FLAG-tagged Virp1 with an estrogen-inducible promoter was co-expressed transiently with TAP-tagged IMPa1 or IMPa-4 *via* agroinfiltration in *N. benthamiana*. Three days post infiltration, 4 mM 17-b-estradiol was infiltrated in leaves 6 h before sampling. The cell lysates from leaf samples were incubated with anti-FLAG antibody (catalog #MA1-142; Thermo Fisher Scientific) for 1 h at 4°C. The magnetic protein A/G beads (catalog #88802; Thermo Fisher

Scientific) were then added to the lysate for another 1 h incubation at 4°C with mild shaking. The beads were washed twice with 1X PBST buffer (137 mM NaCl, 2.7 mM KCl, 10 mM Na2HPO4, 1.8 mM KH2PO4, 0.1% Triton X-100) and once with distilled water. The bound proteins were eluted using IgG elution buffer (Thermo Fisher Scientific) and then subject to immunoblots. Co-IP experiments have been repeated twice. For each biological replicate, mixed leaf tissues from three or more plants were used for each treatment.

3.2.5 Protein purification

GST and Recombinant Virp1-GST proteins were expressed in Escherichia coli Rosetta strain (EMD Millipore, Burlington, MA). Cells were grown overnight at 37°C in LB media supplied with ampicillin (100 µg/mL) and chloramphenicol (34 µg/mL). An aliquot of cells with OD600 = 0.1 was inoculated into fresh LB supplied with antibiotics the next day. Once the cell density (OD600) reached 0.5-0.7, 0.4 mM IPTG (final concentration) was added to the culture to induce protein expression. After inducing at 20°C overnight, 100 mL culture was harvested by centrifugation at 8,000 rpm for 8 min. Pellets were re-suspended in 1X PBS buffer (137 mM NaCl, 2.7 mM KCl, 10 mM Na_2HPO_4, and 1.8 mM KH_2PO_4) supplement with 20 mM PMSF and sonicated to lyse the cells. The cell lysate was then centrifuged at 10,800 rpm for 30 min at 4°C. The supernatant was collected and incubated for 1 h with 2 mL of 50% slurry of Glutathione Resin (Genscript) before loading onto an empty EconoPac gravity-flow column (Bio-Rad Laboratories, Hercules, CA). The resin was then washed with 10 mL 1xPBS followed by applying 10 mL elution buffer (50 mM Tris-HCl pH 8.0 and 10 mM reduced glutathione). The elutes were concentrated using an Amicon protein concentrator (MilliporeSigma, Burlington, MA). Proteins were then separated by 8% SDS-PAGE electrophoresis followed by Coomassie blue staining and de-staining to estimate concentration using a BSA standard as

reference.

3.2.6 Electrophoresis mobility shifting assays (EMSAs)

The detailed protocol has been reported previously [44]. Binding assays that contained RNA in the absence or presence of different amounts of GST or Virp1-GST proteins were incubated at 28°C for 30 min. The binding buffer was composed of 10 mM HEPES-NaOH (pH 8.0), 50 mM KCl, 100 mM EDTA, and 5% glycerol. Electrophoresis for the binding assay was performed on ice in 6% polyacrylamide (29:1) gels at 140 V using 0.5X TBE (50 mM Tris, 50 mM boric acid, 1 mM EDTA, pH 8.3) for 1.6 h. The following steps are described below in the RNA gel blots section. The percentage of shifted variant RNAs was normalized to that of WT RNAs to infer a relative binding strength to Virp1, based on at least three replicates.

3.2.7 Tissue processing and *in situ* hybridization

The tissue fixation and processing were largely described previously [65] with minor modification. Briefly, *N. benthamiana* leaf samples (8 days post-inoculation) and tomato systemic leaves (3 weeks post-inoculation) were collected and fixed in FAA solution (50% ethanol/5% formaldehyde/5% acetic acid) for 30 min and then dehydrated by a step-wise gradient of ethanol solutions (50%, 80%, 95% and 100%). The samples were washed by 1XPBS and treated with 10 mg/mL of proteinase K for 20 min at 37°C. Then, the samples were hybridized with Dig-labeled antisense riboprobes (generated as above-mentioned) at 50°C overnight. The samples were washed, incubated with anti-DIG monoclonal antibody (catalog #11333089001; MilliporeSigma) and NBT/BCIP substrate (MilliporeSigma) subsequentially, and mounted with Permount (Thermo Fisher Scientific) for visualization using an Olympus CX23 light microscope. The scale bars were calculated using ImageJ (https://imagej.nih.gov/ij/).

Samples from at least four plants were used for each treatment.

3.2.8 RNA gel blots and immunoblots

After electrophoresis, RNAs were then transferred to Hybond-XL nylon membranes (Amersham Biosciences, Little Chalfont, United Kingdom) *via* a semi-dry transfer cassette (Bio-Rad Laboratories) and were immobilized by a UV-crosslinker (UVP, Upland, CA). RNAs were then detected by DIG-labeled UTP probes. AP-conjugated anti-DIG monoclonal antibody (catalog #11333089001; MilliporeSigma) was used in combination with Immun-Star substrates (Bio-Rad Laboratories). Signals were captured by ChemiDoc (Bio-Rad Laboratories).

After SDS-PAGE electrophoresis, we followed the previously described protocol for immunoblotting [89]. IMPas were detected by a monoclonal mouse anti-Myc antibody (catalog #M5546; MilliporeSigma; 1:3,000 dilution). Virp1 was detected by a monoclonal mouse anti-FLAG antibody (catalog #F1804-200UG; MilliporeSigma; 1:1,000 dilution). HRP-conjugated anti-mouse serum (catalog #1706516; Bio-Rad Laboratories) was diluted at 1:2,000. SuperSignal West Dura (Thermo Fisher Scientific) was used as the substrate. Signals were captured by ChemiDoc (Bio-Rad Laboratories).

3.2.9 Bimolecular fluorescence complementation and microscopy

For BiFC, *N. benthamiana* seedlings were used for agroinfiltration of various combinations of constructs, all including 35S:RFP-Histone 2B [129] as the nucleus marker. The N split (aa 1-174) YFP was fused in front of the N-terminus of LHP1 or Virp1. The C split YFP (aa 175-end) was fused after the C-terminus of IMPa-1 or IMPa-4. For GFP-fusion proteins, we used agroinfiltration for expression in *N. benthamiana* seedlings and DAPI staining to indicate the nucleus following our established method [80]. Samples from 10 randomly chosen regions of

infiltrated leaves were analyzed. EVOS FL imaging system (Thermo Fisher Scientific) was used for observing the fluorescence expressed in cells. For GFP channel, we used a fixed setting with lower illumination (30%) and a shorter exposure time (250 ms). LHP1-GFP and Virp1-GFP signals were quantified using ImageJ. The quantification data were analyzed by the unpaired T-test (two-tailed), using the built-in function in Prism (GraphPad Software, LLC).

3.2.10 Data availability

The published RNA-Seq dataset has been deposited in the NCBI SRA with accession number SRP093503. The accession numbers of *A. thaliana* IMPa genes are: At IMPa-1 (AT3G06720), *At* IMPa-2 (*AT*4G16143), *At* IMPa-3 (*AT*4G02150), *At* IMPa-4 (*AT*1G09270), *At* IMPa-5 (*AT*5G49310), *At* IMPa-6 (AT1G02690), *At* IMPa-7 (AT3G05720), *At* IMPa-8 (*AT*5G52000), and *At* IMPa-9 (*AT*5G03070). The accession numbers of tomato (*S. lycopersicum*) IMPa genes are *Sl* IMPa-1 (Solyc08g041890), *Sl* IMPa- 2 (Solyc01g060470), *Sl* IMPa-3 (Solyc06g009750), *Sl* IMPa-4 (Solyc01g100720), and *Sl* IMPa-9 (Solyc10g084270), The accession numbers of *N. benthamiana* IMPa-4 homologs are Niben101Scf01964g10002.1 and Niben101Scf04827g03005.1. The *At VIRP1* gene accession is *AT*5G65630. The accession numbers of PSTVd, HSVd, and Q-satRNA used in this study are AY937179, DQ371459, and J02060, correspondingly.

3.3 Results

3.3.1 IMPa-4 is responsible for PSTVd nuclear import

A.thaliana contains the necessary machinery to support PSTVd nuclear import and replication but repels PSTVd systemic infection [89, 130]. To test whether any IMPa protein(s) is responsible for viroid nuclear import, we employed the RNA-immunoprecipitation assay to

test whether any of the nine Arabidopsis IMPa proteins associated with PSTVd in a complex. We expressed IMPa proteins *via* agroinfiltration in PSTVd-infected *N. benthamiana* plants for the RNA-immunoprecipitation assay. As shown in Figure 3.1, only IMPa-4 could specifically and consistently enrich PSTVd, as revealed by the presence of PSTVd in the immunoprecipitated fractions *via* RT-PCR. We chose Histone H2A mRNA (Niben101Scf01866g00004.1) as a negative control for RT-PCR because mRNAs cannot traffic back to the nucleus. Moreover, the H2A ortholog in tomato did not change expression level in PSTVd- or virus-induced gene silencing vector (tobacco rattle virus; TRV)-infected plants in our previous studies [111, 131]. As shown in Figure 3.1, IMPa-4 did not bind with the Histone H2A mRNA, further supporting the specificity of IMPa-4 in forming a complex with PSTVd. Homology-based analysis found Sl IMPa-4 in tomato (Table A.4), a host of PSTVd. None of the tomato IMPas, including IMPa-4, displayed any significant change in expression in PSTVd-infected leaves in our previously published RNA-Seq data (Table A.4).

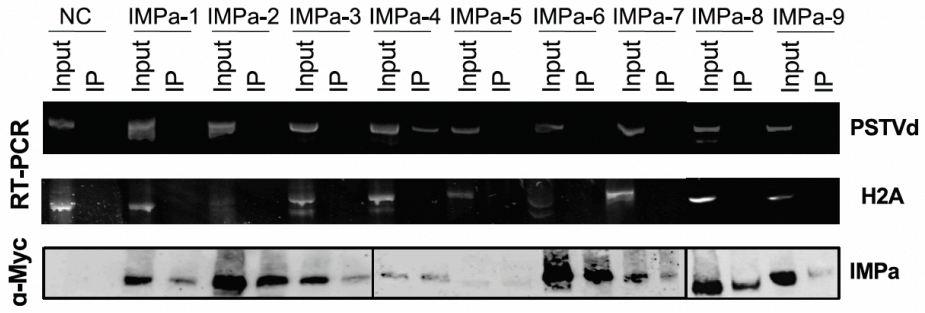

Figure 3.1 RNA immunoprecipitation.

IMPa genes were fused with a TAP-tag, which contains 9X cMyc, 2X IgG binding domain, and 1X His6. IMPa genes were transiently expressed in PSTVd-infected *N. benthamiana* plants *via* agroinfiltration and then harvested for immunoprecipitation using magnetic IgG beads. RNAs in the immunoprecipitation were subject to RT-PCR followed by electrophoresis using native PAGE gels. Histone H2A serves as a negative control. NC, infiltration with agrobacterium harboring no construct. IP, immunoprecipitated fraction.

We then analyzed the IMPa homologs in tomato, a host plant of PSTVd and identified five genes: Sl *IMPa-1*, Sl *IMPa-2*, Sl *IMPa-3*, Sl *IMPa-4*, and Sl *IMPa-9* (Table A.4). Their expression was not significantly changed by infection of PSTVd or TRV vector (Table A.4) [111, 131]. Therefore, we employed the virus-induced gene silencing assay to specifically down-regulate the expression of Sl IMPa-4 and tested PSTVd infection therein to corroborate the role of IMPa-4 in PSTVd infection, The TRV^{GFP} served as a control that did not affect PSTVd infectivity (Figure 3.2). We cloned an IMPa-4-specific fragment based on the BLAST result and constructed TRV^{IMPa-4}. As expected, the TRV^{IMPa-4} construct transiently suppressed IMPa-4 expression, which led to great reduction of PSTVd accumulation in systemic leaves (Figure 3.2). Whole-mount *in situ* hybridization analyses of the systemic leaves from PSTVd and TRV^{IMPa-4} co-infected plants could detect very few PSTVd-infected nuclei therein, which contracts with the presence of numerous PSTVd-infected nuclei in the systemic leaves co-infected with PSTVd and TRV^{GFP} (Figure 3.3). We analyzed samples from four TRV^{GFP}-infected and five TRV^{IMPa-4}-infected plants and found the difference is statistically significant with a P value below 0.0001 (Figure 3.3). These data suggested that IMPa-4 likely facilitates viroid nuclear imports in plants.

3.3.2 Virp1 interacts with IMPa-4 for nuclear import

Virp1 was discovered through screening a cDNA library from PSTVd-infected tomato for RNA ligand binding [45] and was shown to affect viroid trafficking [132] and replication [133]. Down-regulation of Virp1 expression is known to attenuate viroid replication in cells [133]. Recent progress showed that Virp1 is responsible for the nuclear import of Q-satRNA [42]. However, whether Virp1 is responsible for viroid nuclear import remains elusive. If so is true, Virp1 will likely function in the same pathway as IMPa-4.

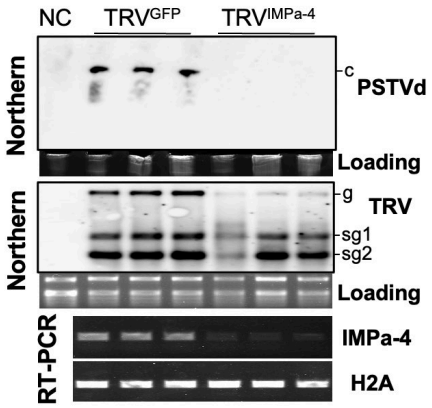

Figure 3.2 Virus-induced gene silencing of IMPa-4 inhibiting PSTVd systemic infection in tomato.

RNA gel blots showing PSTVd and TRV accumulation in infiltrated leaves. RT-PCR showing the specific downregulation of IMPa-4 by the TRV^{IMPa-4} construct. c depicts circular genomic PSTVd. G, sg1, and sg2 indicate the genomic RNA1, subgenomic1 from RNA1 and subgenomic2 from RNA1, respectively. NC, wild type tomato without PSTVd or TRV inoculation.

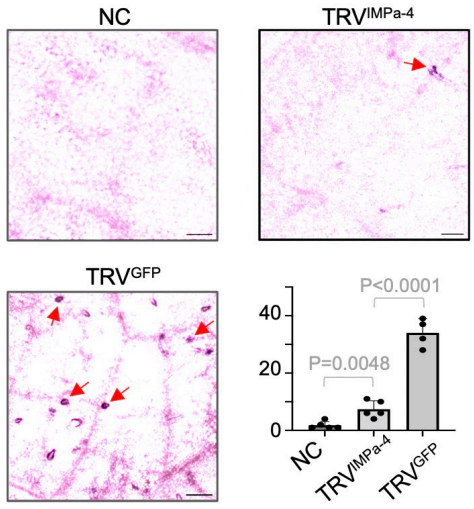

Figure 3.3 Virus-induced gene silencing inhibiting PSTVd nuclear accumulation in systemic leaves.

Whole-mount *in situ* hybridization showed that PSTVd-infected nuclei can only be detected in the systemic leaves of TRV^{GFP} inoculated tomato but not the TRV^{IMPa-4} inoculated tomato. NC, wild type tomato without PSTVd or TRV inoculation. Scale bar, 40 µm. Quantitative analysis of PSTVd-infected nuclei in similar visual areas from 4-5 plants of each treatment. Two-tailed *t*-test was performed using the built-in function in Prism.

To test this possibility, we first analyzed the role of IMPa-4 in regulating Virp1 nuclear import. We infected *N. benthamiana* plants with TRV^{vector} or TRV^{IMPa-4} *via* agroinfiltration. After verifying infection two weeks later (Figure 3.4), we then transiently expressed LHP1-GFP or Virp1-GFP in those plants *via* agroinfiltration. LHP1 (LIKE HETEROCHROMATIN PROTEIN 1) relies on the redundant function of IMPa-1, IMPa-2, and IMPa-3 for nuclear import [118]. As shown in Figure 3.4B, LHP1-GFP displayed similar fluorescence signals between plants infected with TRV^{vector} and TRV^{IMPa-4}. In contrast, Virp1-GFP has relatively higher fluorescence signal in plants infected with TRV^{vector} than those infected with TRV^{IMPa-4} (Figure 3.4B). We quantified fluorescence signals in more than 50 nuclei from 10 randomly picked areas for each treatment and found that the Virp1-GFP signal reduction in TRV^{IMPa-4}-infected plants is statistically significant ($P<0.0001$) based two-tailed t-test (Figure 3.4C).

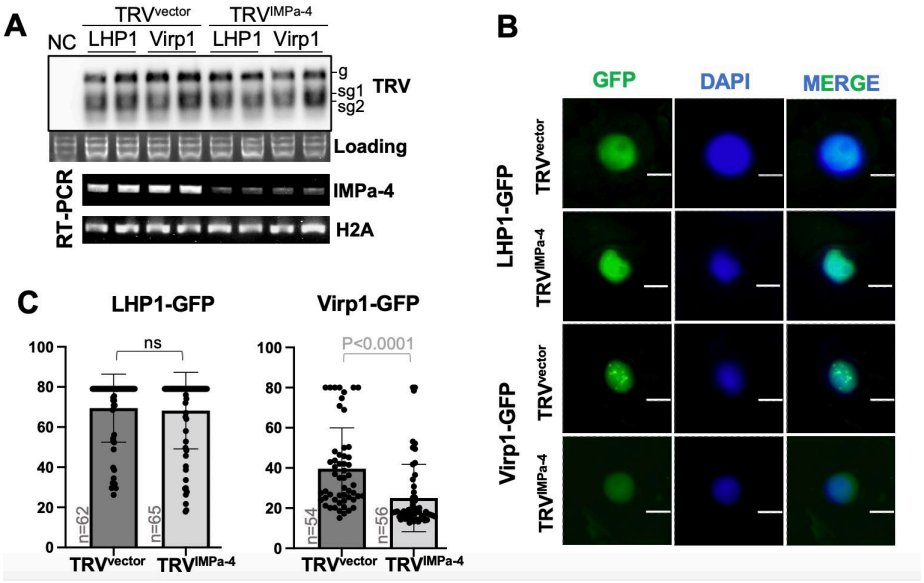

Figure 3.4 Virus-induced gene silencing inhibiting *IMPa-4* expression in systemic leaves of *N. benthamiana* plants (A) and reducing Virp1-GFP but not LHP1-GFP accumulation in the nucleus (B).

Figure 3.4 (continued)

NC, wild type *N. benthamiana* plants without TRV inoculation. DAPI staining marks the nucleus. Scale bar, 8 μm. (C) Statistical analysis of nuclear GFP signal showing that Virp1-GFP but not LHP1-GFP reduced accumulation in the nucleus of plants with suppressed IMPa-4 expression. ns, not significant.

To test the possible physical interactions between IMPa-4 and Virp1, we employed the co-immunoprecipitation assay to test the interaction between these two proteins. Since Virp1 expressed at relatively low level in *N. benthamiana*, we used an estrogen-based inducible expression system [134] to boost the expression of Virp1. We co-expressed a FLAG-tagged Virp1 construct with TAP-tagged IMPa-4 or IMPa-1 *via* agroinfiltration. 17-b-estradiol was then supplied one day before sample collection. As shown in Figure 3.5A, Virp1 interacted with IMPa-4 but not IMPa-1. We also performed BiFC to further confirm the interaction between Virp1 and IMPa-4. As shown in Figure 3.5B, agroinfiltration with a mixture of YFPN-Virp1 and IMPa-4-YFPC in *N., benthamiana* seedlings led to the detectable YFP fluorescence. In contrast, there was no signal in cells co-expressing YFPN-Virp1 and IMPa-1-YFPC (Figure 3.5B). For BiFC assay, we also included LHP1 as an additional control. We observed YFP signal in cells co-expressing YFPN-LHP1 and IMPa-1-YFPC but not cells co-expressing YFPN-LHP1 and IMPa-4-YFPC (Figure 3.5B). Based on the data, Virp1 and IMPa-4 likely form a complex for nuclear import.

3.3.3 A 3-dimensional RNA motif mediates Virp1 binding with PSTVd

Previous analysis suggested that Virp1 binds to two possible RY motifs (R: A or G; Y: C or U) in PSTVd [44], but the structural basis of the RY motif remains elusive. Furthermore, despite that a similar RY motif has been found in another nuclear-replicating viroid HSVd, the

overall structures of the RY motif-containing regions between PSTVd and HSVd displayed significant differences [44].

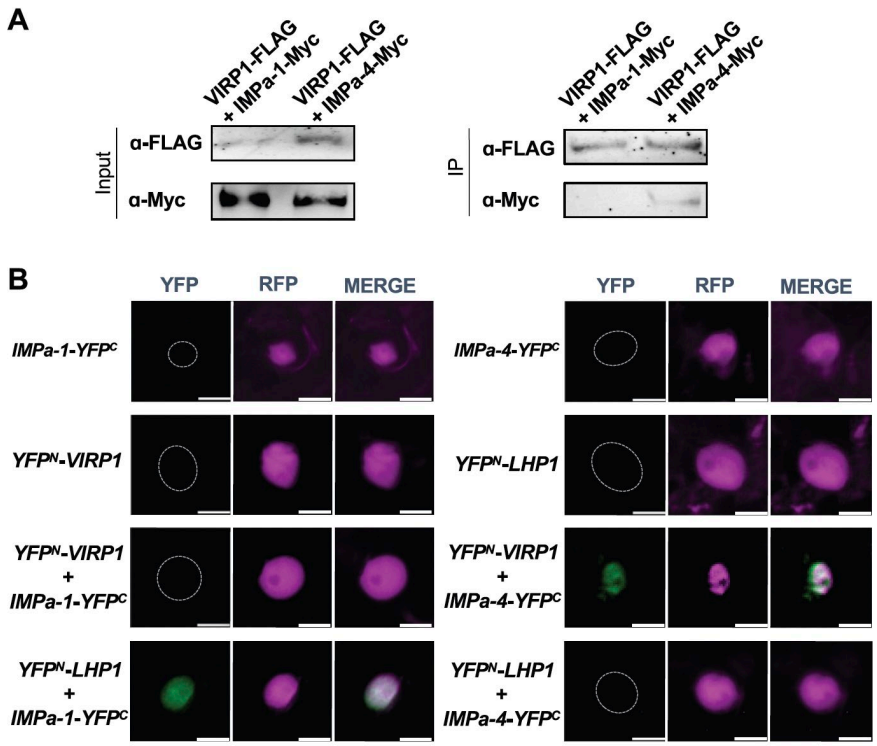

Figure 3.5 IMPa-4 and Virp1 interaction in plants.

(A) Co-immunoprecipitation. Agroinfiltration-based transient expression of FLAG-tagged Virp1 in *N. benthamiana* serves a bait to pull down co-expressed IMPa proteins with a TAP-tag. IP, immunoprecipitated fraction. (B) BiFC. *N. benthamiana* seedlings were used for transient expression of various combinations of constructs *via* agroinfiltration. 35S:RFP-Histone2B serves as a marker for the nucleus. Scale bar, 8 μm. White dashed lines outline the positions of nuclei.

A close look at the region containing RY motifs in PSTVd showed that there is a C-loop (loop 26) (Figure 3.6). C-loop is an asymmetric internal loop, which has the following characteristic features: 1) the first base in the longer strand is often a C with some exceptions; 2) the longer strand has two bases forming non-WC-WC base pairings with bases in the other strand; 3) bases from two strands form two triads; 4) this motif often resides in hairpin stem-loop

structure [47, 49]. Interestingly, our preliminary analysis showed that replacing the C-loop with WC-WC base pairs abolished PSTVd nuclear localization in *in situ* hybridization analysis.

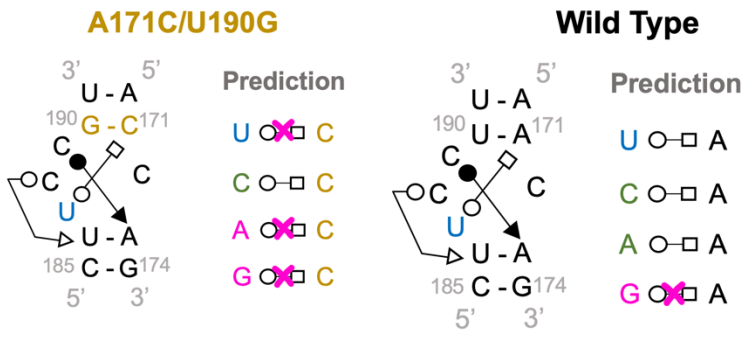

Figure 3.6 Rationale for C-loop mutant designs.

Based on the RNA basepair catalog, structure-maintaining and structure-disruptive mutants were designed and highlighted in green and magenta, respectively.

According to the C-loop model, PSTVd loop 26 is defined by two WC-WC base pairings (A171-U190 and A173-U186) on both ends. Within this potential C-loop, C189-A173 can form a *cis*-WC-Sugar base pair (cWS) and U187-A171 can form a *trans*-WC-Hoogsteen (tWH) base pair. The C189-A173 and U187-A171 base pairs, together with the WC-WC base pairs on both ends, can form two triads (Figure 3.7). C188 and U186 may form a *trans*-WC-Sugar base pair (tWS) as found in some but not all C-loop structures [47, 49]. C172 is predicted as a free-standing base that is not involved in any base-pairing. This PSTVd C-loop model is well supported by the chemical mapping data (Figure 3.7) [33, 36, 135]. Selective 2′ Hydroxyl Acylation analyzed by Primer Extension (SHAPE) assays from multiple studies using different chemicals collectively showed that C172 is highly reactive to modification *in vitro* and *in vivo* (Figure 3.7), indicating that it is not involved in base-pairing. In contrast, C189 consistently showed low reactivity in both *in vitro* and *in vivo* mapping assays (Figure 3.7), indicating that it

is involved in base-pairing. U187 showed medium reactivity in some of the mapping assays but low reactivity in others, which may be attributed to the loop "breathing" effect [136]. In fact, this is in agreement with the observation that the partner of U187, A171, also showed relatively high reactivity in some mapping experiments (Figure 3.7). In summary, extensive chemical mapping experiments essentially support that PSTVd loop 26 is a C-loop.

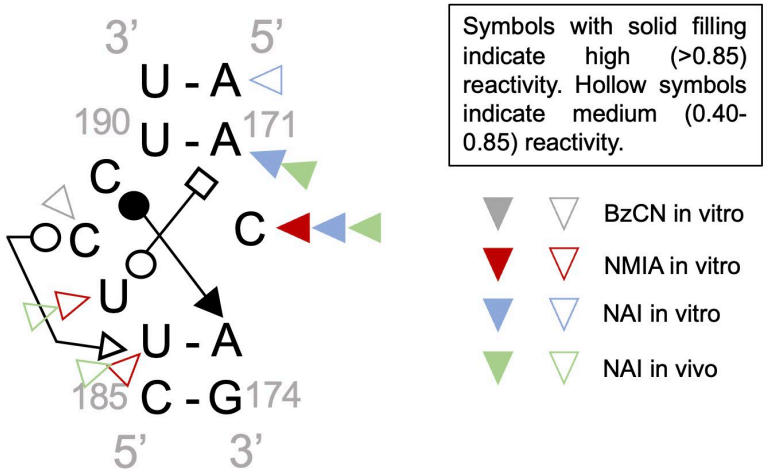

Figure 3.7 Selective 2' Hydroxyl Acylation analyzed by Primer Extension (SHAPE) analyses support PSTVd C-loop model.

The figure plotted using the published data [33, 137]. Bases with low reactivities were not highlighted. BzCN, Benzoyl Cyanide. NMIA, N-methylisatoic anhydride. NAI, 2-methylnicotinic acid imidazolide.

We employed mutational analyses to further test whether loop 26 is a C-loop. Within the PSTVd C-loop (Figure 3.6), the *c*WS base-pairing between C189 and A173 as well as the *t*WS base-pairing between C188 and U186 are flexible for any nucleotide substitution in theory according to the RNA Basepair Catalog [120], so mutations in these two base pairings may not lead to any conclusive result. Instead, we designed substitutions to replace U187 that may or may not maintain similar *t*WH base-pairing with A171. Alternatively, we replaced the U190-A171

cis-WC-WC base pair with G190-C171. Under this condition, U187 can only be substituted by C187 to maintain the tWH interaction with C171 according to the RNA Basepair Catalog. Using these mutational variants, we performed electrophoretic mobility shift assays (EMSAs) using recombinant Virp1. Interestingly, Virp1 only displayed a strong binding to WT PSTVd in EMSA (Figure 3.8A and 3.8B). Among all the tested variants, all structure-maintaining variants have relatively stronger binding to Virp1 as compared with structure-disruptive variants (Figure 3.8B).

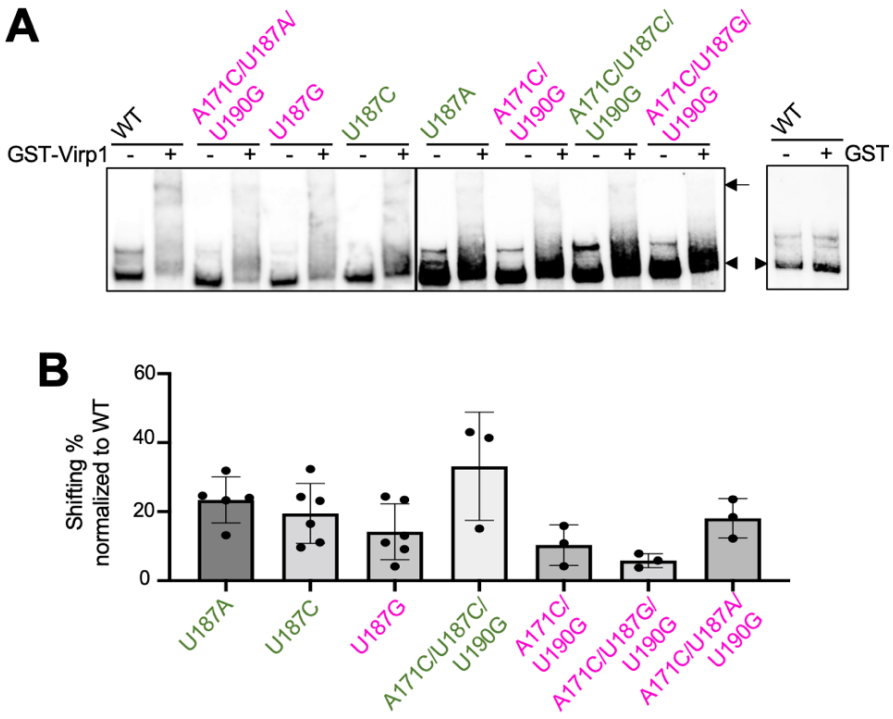

Figure 3.8 Characterizing PSTVd C-loop.

(A) EMSA illustrating the interaction between C-loop mutants and Virp1. Arrows and arrow heads indicate shifted RNA (in RNA-protein complex) and free RNA, respectively. (B) Box plot showing quantification of EMSA results. The percent of RNA shifted in total RNA used for each reaction was calculated. The WT RNA shifted percentage was set as 100% in each replicate, and the mutant RNA shifted percentage was normalized to that of WT RNA. All C-loop mutants have a significant reduction in Virp1-binding as compared with WT, based on two-tailed *t*-test.

3.3.4 C-loop is critical for the infectivity and nuclear import of PSTVd

In attempt to determine the biological functions of C-loop in PSTVd, we analyzed the infectivity of C-loop mutants. As shown in Figure 3.9, all PSTVd C-loop disruptive variants and one structure-maintaining mutant (A171C/U187C/U190G) failed to systemically infect *N. benthamiana*. All these infection defective mutants have a weaker binding to Virp1. Two structure-maintaining mutants, U187A and U187C, showed systemic infection. A careful analysis of the RNA progeny in the systemic leaves revealed that none of the progeny maintained the original sequences as inoculum (Table A.6). Nevertheless, nuclear localization is the prerequisite to initiating replication before mutations occur. Therefore, our data support that the PSTVd structure-maintaining mutants U187A and U187C probably possess the ability to enter the nucleus. Importantly, the data support that PSTVd loop 26 is a C-loop, because only the variants predicted to maintain the C-loop structure have relatively stronger binding with Virp1 and retain the capacity to initiate replication.

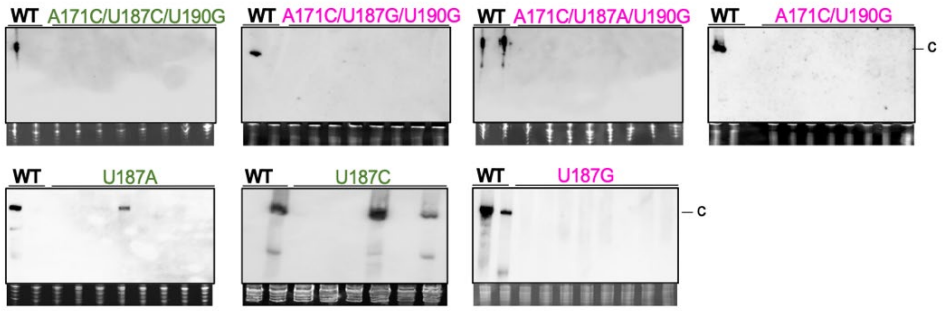

Figure 3.9 RNA gel blots detecting the PSTVd systemic infection in *N. benthamiana*. WT PSTVd serves as positive control. Ethidium bromide staining of rRNAs serve as loading control. c, circular PSTVd.

We then analyzed the local leaves inoculated with C-loop variants *via* whole-mount *in situ* hybridization because it has been well established that viroid-infected nuclei can be visualized by this method thanks to the high concentration of viroid RNAs [58, 65, 105, 138]. As shown in Figure 3.10, very few signals could be detected in local leaves inoculated with C-loop disruptive variants (*i.e.*, U187G, A171C/U190G, A171C/U187A/U190G, A171C/U187G/U190G). Those signals are likely background false-positives akin to those in the non-inoculated control leaves because the signals in C-loop mutants and in negative controls have no significant differences in *t*-test (*P* – values all above 0.3) (Figure 3.10). The structure-maintaining mutants (U187A and U187G) were not included in this assay because we cannot distinguish the original inoculum and replication products with mutations in whole-mount *in situ* hybridization assay. In contrast, WT PSTVd resulted in significantly more signals of infected nuclei than any of the mutant-inoculated samples (P values all below 0.0005) (Figure 3.10). In addition, the replication-defective A261C mutant of PSTVd, which still has nuclear import ability [121], showed detectable nuclear accumulation as well (Figure 3.10). The nuclear accumulation signal of A261C in Whole-Mount *in situ* hybridization demonstrated that this assay is sensitive enough to capture imported inoculum without replication. The lack of signal of C-loop disruptive variants is unlikely caused by RNA stability, as we often observed C-loop variant inoculums in the local leaves 10 days post-infection.

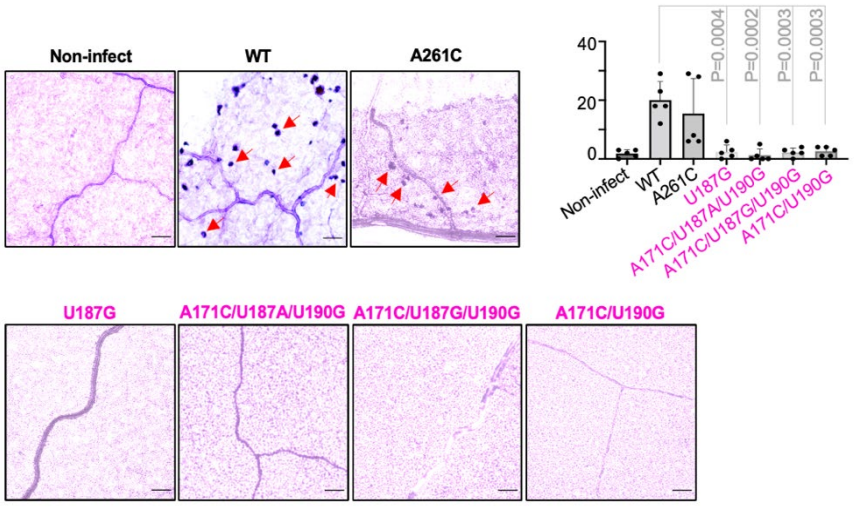

Figure 3.10 Whole-mount *in situ* hybridization showing the presence of viroid RNAs in nuclei (purple dots).

Scale bars, 72 μm. Red arrows indicate examples of PSTVd-accumulated nuclei. Quantitative and statistical analyses of PSTVd-infected nuclei in similar visual areas from 4 plants of each treatment. There is no significant difference between noninfected and any of the C-loop mutant samples (*P*-value all > 0.3).

To further test RNA stability, we used agroinfiltration to deliver the cDNAs of C-loop variants into *N. benthamiana* plants. We detected their accumulations about 3-fold stronger than the A261C transcripts and slightly lower than the WT (Figure 3.11). Altogether, the Whole-Mount *in situ* hybridization results supported that the C-loop disruptive variants lost their nuclear import ability. Taken together, our data indicate that the C-loop plays an important role in nuclear import and full infectivity of PSTVd.

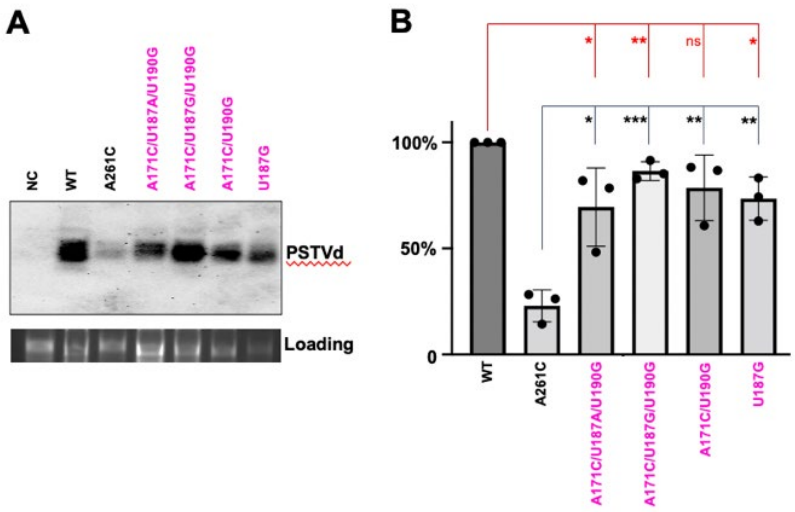

Figure 3.11 The RNA stability of PSTVd C-loop variants.

C-loop mutants, in comparison to wild type (WT) and A261C mutant, were transiently expressed in *N. benthamiana via* agroinfiltration using CaMV 35S promoter driven RZ:Int-based constructs. (A)Total RNAs purified from 4 days post infiltration leaves were run in 2% agarose gel and blotted with PSTVd specific ribo-probes. Ethidium bromide staining of rRNAs serves as loading control. NC, leaves infiltrated with agrobacteria harboring no construct. (B) Quantification of the PSTVd WT and mutant RNA abundance from three biological replicates. The signal of WT PSTVd RNA was set as 100%. Two-tailed *t*-tests were performed for pairwise comparison of C-loop mutant RNAs with WT or A261C using the built-in function in Prism. *, **, and *** dictate P values below 0.05, 0.01, and 0.001, respectively. “ns” means not significant. Magenta color depicts structure-disruptive mutants.

3.3.5 C-loop widely exists in nuclear-replicating viroids

Notably, C-loop can be found in 27 out of 28 formal members and three candidate members of the family *Pospiviroidae* (Figure 3.12). Based on sequence variations and genomic coordination, we can categorize those viroids into two groups (Figure 3.12). Interestingly, there are 11 viroids, including PSTVd, containing exactly the same C-loop with identical genomic localization. The remaining 19 viroids in Figure 3.12 have C-loop structures with diverse sequence variations and genomic localization patterns, which still fit the C-loop model. This observation indicates that C-loop is likely a common motif exploited by viroids for nuclear import.

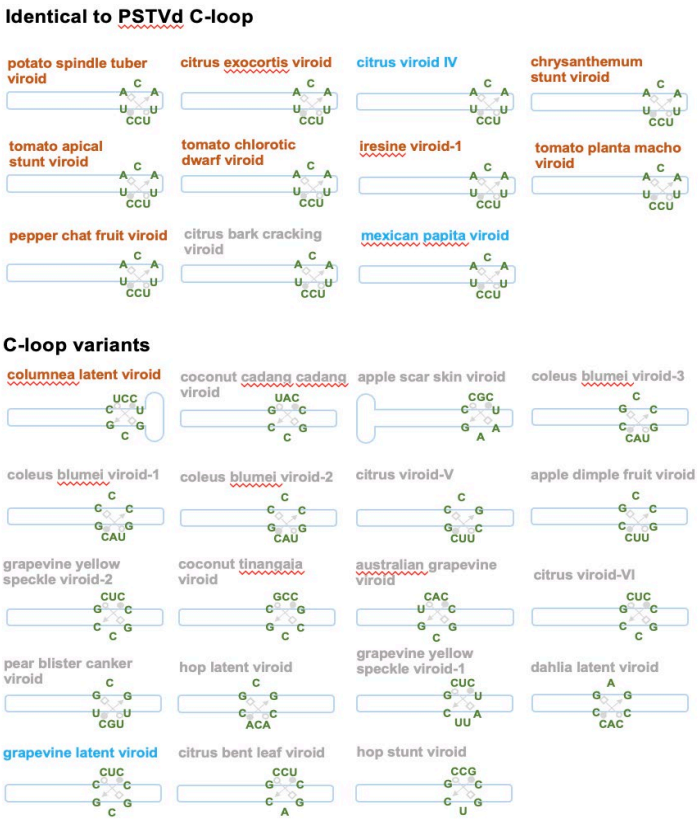

Figure 3.12 C-loop in nuclear-replicating viroids.

Illustration of viroid C-loop sequences and relative genomic loci Viroids shown in brown belong to the genus *Pospiviroid*. Viroids shown in blue were considered but not confirmed as members of the family *Pospiviroidae* in the latest taxonomy.

Notably, we also found a variant version of C-loop in HSVd (Figure 3.13A), a PSTVd relative that has a slightly weaker binding to Virp1 [45]. To test this C-loop variant, we replaced the C128-G172 *cis*-WC–WC base pair with G–C, A–U, or U–A (Figure 3.13A). Only the A128-U172 substitution is predicted to disrupt the tWH base pair within the C-loop. Again, all HSVd C-loop mutants, including one structure-disruptive and two structure-maintaining mutants, exhibited much-reduced binding to Virp1 (Figure 3.13, B and C). Both structure-maintaining mutants exhibited a slightly stronger binding to Virp1 as compared with the structure-disruptive mutant. Since we observed reduced binding in all the mutational designs, one more mutant

(G157C), which affects an adjacent loop to the C-loop in HSVd, was included as a control. This mutant now had significantly stronger binding to Virp1 as compared with the binding between Virp1 and HSVd C-loop mutants (Figure 3.13, B and C).

When we used HSVd C-loop variants and the G157C mutant to infect *N. benthamiana* plants, only G157C can accomplish successful infection (Figure 3.13D). Sequencing of the progeny confirmed that the G157C mutation was retained in the progeny in systemic leaves (Table A.6). Altogether, our observation supports that C-loop is critical for HSVd infectivity and Virp1 specifically recognizes HSVd C-loop. Since our structure-maintaining mutants also showed weak binding to Virp1, it implies the existence of additional selection pressure that prefers certain nucleotides in composition of the C-loop.

3.4 Discussion

Proper subcellular localization dictates the function of biomolecules, including various cellular and infectious RNAs. While a majority of cellular RNAs are generated in the nucleus and then either stay in the nucleus or are transported to the cytoplasm for function, more and more RNAs were found to traffic in the reverse direction from the cytoplasm to the nucleus participating in diverse biological processes [5, 38-42, 139].

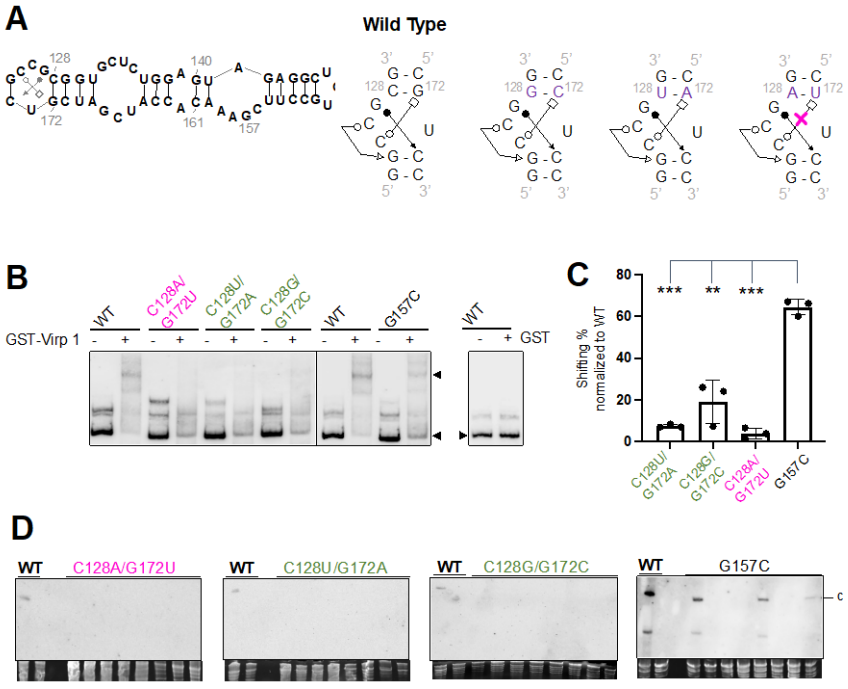

Figure 3.13 Characterizing a C-loop variant in HSVd.

(A) Rationale for HSVd C-loop mutagenesis. The critical *trans*-WC–Hoogsteen base pairing between C125 and G172 is subject to mutagenesis. Based on the RNA basepair catalog, C125–G172, C125–C172, C125–A172 but not C125–U172 can form the critical *t*WH pairing. The magenta cross depicts the structure-destructive design. (B) EMSA illustrating the interaction between C-loop mutants and Virp1. Arrowheads indicate the position of free probe, while the arrow indicates the position of RNA–protein complex. Multiple bands in "RNA only" lanes are likely caused by different confirmations of RNAs. (C) Box plot showing quantification of EMSA results. Normalization method was the same as described in Figure 3.8. All C-loop mutants have a significant reduction in Virp1 binding as compared with WT and G157C RNA, based on two-tailed *t* test. $^{**}P < 0.1$. $^{***}P < 0.001$. (D) RNA gel blots detecting HSVd systemic infection in *N. benthamiana*. WT HSVd serves as positive controls. Ethidium bromide staining of rRNAs serves as loading control. c, circular genomic HSVd. Green and magenta colors depict structure-maintaining and structure-disruptive mutants, respectively.

However, the mechanism underlying RNA nuclear import is poorly understood. Here, we present evidence supporting that interacting with cellular protein Virp1 through C-loop is critical for transporting pathogenic noncoding RNAs (*i.e.*, viroids) from the cytoplasm to the nucleus in plants (Figure 3.14).

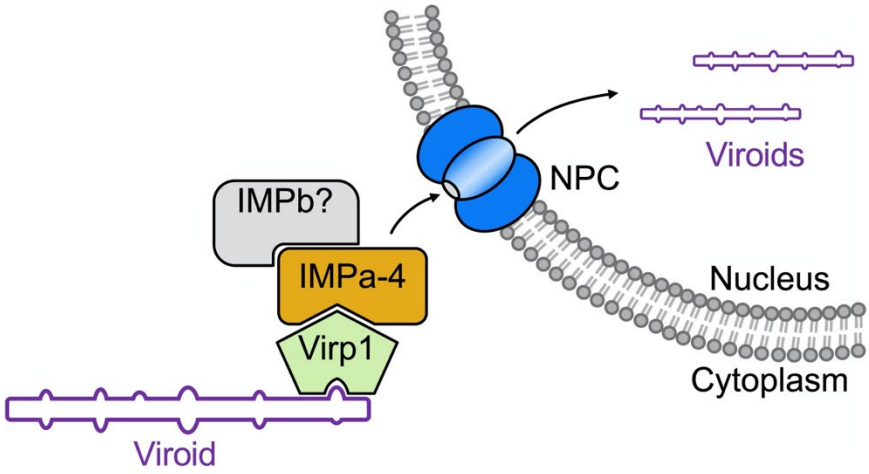

Figure 3.14 A working model illustrating the IMPa-4/Virp1/C-loop-based RNA nuclear import. Virp1 recognizes viroid C-loop to form an RNP complex, which is transported into the nucleus by IMPa-4. The IMPb responsible for viroid nuclear import remains to be identified.

Notably, we identified one genetic element, an RNA C-loop, as a critical signal for viroid nuclear import. PSTVd C-loop model is supported by chemical mapping data (Figure 3.2) and functional mutagenesis analyses. Disrupting C-loop decreased binding with Virp1, reduced nuclear accumulation, and compromised infectivity. The absence of nuclear signal in Whole-Mount *in situ* hybridization using C-loop mutant inoculated samples is unlikely caused by RNA stability because C-loop mutant RNAs have much higher accumulation levels than the A261C mutant, which can be detected in the nuclei in Whole-Mount *in situ* hybridization (Figure 3.10). Previous studies suggest that Virp1 recognizes RY motifs in viroids [44, 45]. RY motif and C-loop partially overlap in some viroids, such as in PSTVd. The drastic changes in binding and infectivity caused by point mutations in PSTVd C-loop support the essential role of C-loop for Virp1 recognition. More importantly, HSVd C-loop disruptive mutants that are not overlapping with RY motifs have a strong effect on infectivity and Virp1-binding. In contrast, the G157C

mutant that overlaps with the HSVd RY-motif retains infectivity and Virp1-binding ability. Altogether, our data strongly support C-loop as a bona fide signal for selective nuclear import of RNA.

C-loop has been found in many rRNAs [47, 49], a bacterial mRNA [46], and some conserved mammalian noncoding RNAs [48]. In general, C-loop increases the local helical twist of RNA helices [140]. Besides, C-loop in the mRNA and those mammalian noncoding RNAs are involved in translational regulation [46, 48]. Our data not only expand the function of the C-loop and but also uncover a new protein partner (*i.e.*, Virp1) for this RNA motif.

There are 28 formal members of the family *Pospiviroidae* [141], and 27 of them (except citrus dwarfing viroid) possess a C-loop. Eleven viroids, including eight out of nine members in the genus *Pospiviroid* which PSTVd belongs to, possess an identical C-loop in their genomes. Interestingly, rest of the viroids of the family *Pospiviroidae* also carry a C-loop, with some variations in sequences and genome localization, except citrus dwarfing viroid (Figure 3.12). Notably, these viroid genomic structures are supported by SHAPE analyses [33-35], except for citrus bark cracking viroid and citrus viroid-VI whose structures were predicted using mFOLD [142]. Therefore, a conserved nuclear import signal likely exists in nearly all nuclear-replicating viroids. Moreover, C-loop variants can also be found in mexican papita viroid, citrus viroid-IV, and grapevine latent viroid, which are candidate members of *Pospiviroidae*. Future functional investigation on those C-loop variants can provide insights into the precise structural basis and critical nucleotide preferences in mediating RNA nuclear import. It is also interesting to analyze citrus dwarfing viroid to test 1) whether it possesses an alternative binding site for Virp1 and/or 2) whether there is an alternative nuclear import route.

Notably, Q-satRNA appears to have a C-loop in its RNA sequence as well. EMSA testing using a C-loop disruptive Q-satRNA showed significantly reduced binding to Virp1 as compared with that of WT Q-satRNA ($P = 0.0012$), further supporting the critical role of C-loop in binding with Virp1 (Figure 3.15). Therefore, C-loop-based RNA nuclear import is possibly exploited by infectious RNAs in common. Whether any cellular RNA follows this pathway for nuclear import to exert functions in plants deserves future investigation. Our study paves the way to explore RNA nuclear import machinery and outlines a model for structural motif-based RNA subcellular localization. This line of research may lead to a comprehensive understanding of the accurate localization of RNAs in cells and future manipulation of subcellular localizations of various RNAs for functional studies and applications.

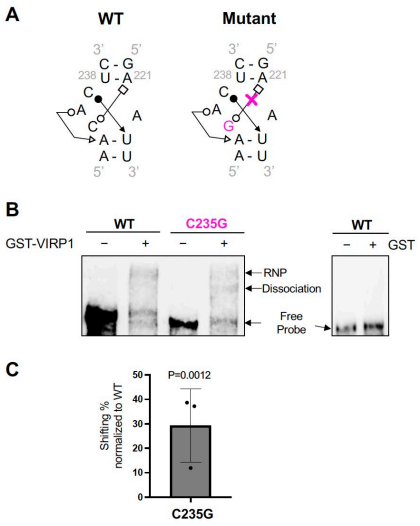

Figure 3.15 Virp1 interaction with Q-satRNA.

(A) Rationale for the C-loop mutant design. Based on the RNA basepair catalog, C235-A221 but not G235-A221 can form the critical *t*WH pairing. (B) EMSA illustrating that C-loop disruptive mutant C235G significantly reduced QsatRNA binding with Virp1. (C) Box plot showing quantification of EMSA results. Quantification method was the same as listed in Figure 3.1. The C235G mutant has a significant reduction in Virp1-binding as compared with wild type (WT) RNA (set as 100% in each replicate), based on two tailed t-test. Magenta color depicts structure-disruptive mutants.

CHAPTER IV

PERSPRCTIVE

This chapter is a modified version of "Emerging value of the viroid model in molecular biology and beyond" published in Virus Research [143] and has been reproduced here with the permission of the copyright holder. I have played a major role in developing the concepts in this chapter.

4.1 RNA structure-mediated viroid trafficking

Due to their noncoding nature, viroids rely on their RNA structures to harness host factors for infection. Genome-wide analysis on PSTVd local motifs found that many RNA loop structures are critical for either replication or systemic trafficking [61]. Detailed analyses have uncovered the function of those trafficking-related loops in regulating nuclear import and spreading across various cellular boundaries.

4.2 RNA structure-mediated nuclear import

It is well known that members of *Pospiviroidae* enter the nucleus for replication [25]. Recently, we identified a critical C-loop for viroid nuclear imports. C-loop is the binding site for Virp1, a known host factor for viroid infection [144]. Previous studies suggest that Virp1 recognizes at least one of the two RY motifs in PSTVd [145]. RY motif appears to be conserved in members of *Pospiviroidae*. We found the PSTVd C-loop partially overlaps with the RY motif closer to the right terminus [43]. Point mutation in PSTVd C-loop strongly impair PSTVd

infectivity, nuclear accumulation, and interaction with Virp1. We also found a C-loop in HSVd, which is not overlapping with the described RY motif therein. Point mutations in HSVd C-loop also strongly impair HSVd infectivity and interaction with Virp1, supporting that C-loop is the *bona fide* binding site of Virp1 [43]. C-loop can be found in nearly all, except one, formal members of *Pospiviroidae* [43] and even in a statellite RNA of cucumber mosaic virus that relies on Virp1 for nuclear import [42]. Altogether, my work provides conclusive evidence demonstrating that C-loop is probably a conserved signal regulating the nuclear import of plant subviral RNAs.

4.3 RNA structure-mediated systemic infection

In a simplified view, viroids need to move from leaf epidermis, through palisade mesophyll and spongy mesophyll, to cross bundle sheath and enter phloem for systemic trafficking. Viroids will also need to cross bundle sheath and invade mesophyll and epidermis in systemic leaves [14]. Strikingly, PSTVd possesses at least one RNA motif regulating the trafficking across most of these tissues. The right terminal loop is critical for movement from epidermis to mesophyll [62]. Loops 6 and 19 both regulate trafficking from palisade mesophyll to spongy mesophyll [66, 146]. Loop 7 dictates the phloem entry from bundle sheath [58]. A bipartite motif controls phloem exiting to bundle sheath in systemic leaves [56]. An emerging model from these data outlines that distinct RNA structural motifs contain the necessary information for crossing various checkpoints between diverse tissue types.

4.4 Viroid interaction with host RNA silencing machinery

Based on the current model, the replication of viroids will generate double-stranded intermediates that will be cleaved by various Dicer-like proteins (DCLs) in plants [90].

Noteworthy is that the PSTVd RNA genome without replication can also be a target of DCLs purified from plants [93]. In general, DCL2 and DCL3 synergistically suppress PSTVd infection, whereas DCL4 somehow positively regulates PSTVd replication in *Nicotiana benthamiana* [91, 92]. Viroid-derived sRNAs can be loaded into Argonaute proteins (AGOs) for function [93, 94]. Specifically, *Agrobacterium tubefaciens*-mediated transient expression of *Arabidopsis* AGOs followed by RNA-immunoprecipitation revealed that plant AGO1, AGO2, AGO3, AGO4, AGO5, AGO8, and AGO9 all can recruit vd-sRNAs. AGO1, AGO2, and AGO3 favor the binding of 21- and 22-nt vd-sRNAs, while AGO4, AGO5, and AGO9 enrich a good portion of 24-nt vd-sRNAs. Interestingly, ectopic expression of AGO1, AGO2, AGO4, or AGO5 attenuated PSTVd titers in infected *N. benthamiana*, supporting their roles in plant-viroid interactions [94].

4.5 Viroid interaction with plant innate immunity

Plants generally deploy a two-layer immunity defending various pathogens, namely pathogen-associated molecular patterns (PAMPs)-triggered immunity (PTI) and effector-triggered immunity (ETI) [147]. PTI functions mainly at cell surface, whereas ETI largely occurs within cells. The orchestrated PTI and ETI activities are essential for plant survival.

The framework that the presence of viroids can trigger host immune responses has been established recently [101, 110, 148]. How can plant cells sense the presence of foreign RNAs (i.e., viroids) and activate the innate immune system remains obscure. Previously it was thought that plants utilize PKV (protein kinase, viroid-induced), a double-stranded-RNA-binding protein kinase, to sense viroid RNAs and triggers defense signaling [149, 150]. However, this PKV appears to be a pseudogene based on comprehensive RNA-Seq analyses [101, 110]. Viroids may not trigger PTI response because they enter host cells mainly through wounding or, to a lesser extent based on current knowledge, insect vectors [151]. Within the infected plants, viroids move

through plasmodesmata [55]. Therefore, viroids are rarely present on cell surface to elicit PTI. Whether viroids can activate ETI is a puzzle because an R gene that can specifically sense viroids has not been found. If viroid does not trigger ETI response, then the immune responses elicited by viroids might be attributable to damage-associated molecular pattern-triggered immunity that was activated by the emission of cell damage related signal molecules yet-to-be-identified [152-154]. Interestingly, a recent study showed that PSTVd replication can lead to up-regulation of miR398-regulated production of reactive oxygen species [155, 156], which may link the activity of RNA silencing and innate immunity in defending viroids. It will be critical to elucidate the detailed mechanism underlying the regulation of miR398 and the detailed events along this regulatory cascade in viroid-infected plants. Undoubtedly, the efforts to understand the viroid-triggered immune response will shed light on the mechanism for plants to perceive the presence of foreign RNAs. Chapter II attempts to identify the responsible genes underlying Arabidopsis non-host resistance may help future investigations along this line of research.

4.6 Future perspectives

Viroids serve as a productive model to delineate RNA structure-function relationships. The function of many PSTVd RNA motifs has been illustrated, and some of them have been studied in detail in terms of structures and cognate factors. It is particularly interesting to expand similar analyses to other viroids, and even RNA viruses, to establish a general view of RNA motif organizations for effective infection. In parallel, it is an exciting area to study the interaction between viroids and host innate immunity. RNAs represent a universal component in all pathogens, yet their direct interactions with plant innate immunity are often overlooked. The viroid model can be useful to advance our understanding of plant innate immunity in terms of sensing foreign RNAs, including but not limited to viruses and viroid.

REFERENCES

1. Ma, J. and Y. Wang, *Studies on Viroid Shed Light on the Role of RNA Three-Dimensional Structural Motifs in RNA Trafficking in Plants.* Front Plant Sci, 2022. **13**: p. 836267.

2. Ding, B. and Y. Wang, *Viroids: uniquely simple and tractable models to elucidate regulation of cell-to-cell trafficking of RNA.* DNA Cell Biol, 2009. **28**(2): p. 51-6.

3. Ding, B., A. Itaya, and Y. Qi, *Symplasmic protein and RNA traffic: regulatory points and regulatory factors.* Curr Opin Plant Biol, 2003. **6**(6): p. 596-602.

4. Liu, L. and X. Chen, *Intercellular and systemic trafficking of RNAs in plants.* Nat Plants, 2018. **4**(11): p. 869-878.

5. Ye, R., et al., *Cytoplasmic assembly and selective nuclear import of Arabidopsis Argonaute4/siRNA complexes.* Mol Cell, 2012. **46**(6): p. 859-70.

6. Axtell, M.J., *Classification and comparison of small RNAs from plants.* Annu Rev Plant Biol, 2013. **64**: p. 137-59.

7. Chantarachot, T. and J. Bailey-Serres, *Polysomes, Stress Granules, and Processing Bodies: A Dynamic Triumvirate Controlling Cytoplasmic mRNA Fate and Function.* Plant Physiol, 2018. **176**(1): p. 254-269.

8. Reagan, B.C., et al., *RNA on the move: The plasmodesmata perspective.* Plant Sci, 2018. **275**: p. 1-10.

9. Long, J., et al., *Nurse cell--derived small RNAs define paternal epigenetic inheritance in Arabidopsis.* Science, 2021. **373**(6550).

10. Kim, J.Y., *Regulation of short-distance transport of RNA and protein.* Curr Opin Plant Biol, 2005. **8**(1): p. 45-52.

11. Qin, C., et al., *Involvement of RDR6 in short-range intercellular RNA silencing in Nicotiana benthamiana.* Sci Rep, 2012. **2**: p. 467.

12. Spiegelman, Z., G. Golan, and S. Wolf, *Don't kill the messenger: Long-distance trafficking of mRNA molecules.* Plant Sci, 2013. **213**: p. 1-8.

13. Ham, B.-K. and W.J. Lucas, *Phloem-Mobile RNAs as Systemic Signaling Agents.* Annual Review of Plant Biology, 2017. **68**(1): p. 173-195.

14. Wang, Y. and B. Ding, *Viroids: small probes for exploring the vast universe of RNA trafficking in plants.* J Integr Plant Biol, 2010. **52**(1): p. 28-39.

15. Banerjee, A.K., et al., *Dynamics of a mobile RNA of potato involved in a long-distance signaling pathway.* Plant Cell, 2006. **18**(12): p. 3443-57.

16. Kim, M., et al., *Developmental changes due to long-distance movement of a homeobox fusion transcript in tomato.* Science, 2001. **293**(5528): p. 287-9.

17. Haywood, V., et al., *Phloem long-distance trafficking of GIBBERELLIC ACID-INSENSITIVE RNA regulates leaf development.* Plant J, 2005. **42**(1): p. 49-68.

18. Lin, S.I., et al., *Regulatory network of microRNA399 and PHO2 by systemic signaling.* Plant Physiol, 2008. **147**(2): p. 732-46.

19. Pant, B.D., et al., *MicroRNA399 is a long-distance signal for the regulation of plant phosphate homeostasis.* Plant J, 2008. **53**(5): p. 731-8.

20. Ding, S.W. and O. Voinnet, *Antiviral immunity directed by small RNAs.* Cell, 2007. **130**(3): p. 413-26.

21. Kalantidis, K., et al., *RNA silencing movement in plants.* Biol Cell, 2008. **100**(1): p. 13-26.

22. Chen, X. and O. Rechavi, *Plant and animal small RNA communications between cells and organisms.* Nature Reviews Molecular Cell Biology, 2022. **23**(3): p. 185-203.

23. Yang, L., et al., *m(5)C Methylation Guides Systemic Transport of Messenger RNA over Graft Junctions in Plants.* Curr Biol, 2019. **29**(15): p. 2465-2476 e5.

24. Lough, T.J., et al., *Functional analysis of the 5′ untranslated region of potexvirus RNA reveals a role in viral replication and cell-to-cell movement.* Virology, 2006. **351**(2): p. 455-65.

25. Ding, B., *The biology of viroid-host interactions.* Annu Rev Phytopathol, 2009. **47**: p. 105-31.

26. Gómez, G. and V. Pallás, *Identification of an in vitro ribonucleoprotein complex between a viroid RNA and a phloem protein from cucumber plants.* Mol Plant Microbe Interact, 2001. **14**(7): p. 910-3.

27. Owens, R.A., M. Blackburn, and B. Ding, *Possible involvement of the phloem lectin in long-distance viroid movement.* Mol Plant Microbe Interact, 2001. **14**(7): p. 905-9.

28. Gomez, G. and V. Pallas, *A long-distance translocatable phloem protein from cucumber forms a ribonucleoprotein complex in vivo with Hop stunt viroid RNA.* J Virol, 2004. **78**(18): p. 10104-10.

29. Takeda, R. and B. Ding, *Viroid intercellular trafficking: RNA motifs, cellular factors and broad impacts.* Viruses, 2009. **1**(2): p. 210-21.

30. Wang, T., et al., *RNA Motifs and Modification Involve in RNA Long-Distance Transport in Plants.* Front Cell Dev Biol, 2021. **9**: p. 651278.

31. Wang, Y., et al., *RNA 3-dimensional structural motifs as a critical constraint of viroid RNA evolution.* PLOS Pathogens, 2018. **14**(2): p. e1006801.

32. Gast, F.U., et al., *Secondary structure probing of potato spindle tuber viroid (PSTVd) and sequence comparison with other small pathogenic RNA replicons provides evidence for central non-canonical base-pairs, large A-rich loops, and a terminal branch.* J Mol Biol, 1996. **262**(5): p. 652-70.

33. Xu, W., et al., *The use of a combination of computer-assisted structure prediction and SHAPE probing to elucidate the secondary structures of five viroids.* Mol Plant Pathol, 2012. **13**(7): p. 666-76.

34. Giguere, T., C.R. Adkar-Purushothama, and J.P. Perreault, *Comprehensive secondary structure elucidation of four genera of the family Pospiviroidae.* PLoS One, 2014. **9**(6): p. e98655.

35. Giguère, T. and J.P. Perreault, *Classification of the Pospiviroidae based on their structural hallmarks.* PLoS One, 2017. **12**(8): p. e0182536.

36. López-Carrasco, A. and R. Flores, *Dissecting the secondary structure of the circular RNA of a nuclear viroid in vivo: A "naked" rod-like conformation similar but not identical to that observed in vitro.* RNA Biol, 2017. **14**(8): p. 1046-1054.

37. Khisamutdinov, E.F., B.A. Sweeney, and N.B. Leontis, *Context-sensitivity of isosteric substitutions of non-Watson-Crick basepairs in recurrent RNA 3D motifs.* Nucleic Acids Res, 2021. **49**(16): p. 9574-9593.

38. Rudt, F. and T. Pieler, *Cytoplasmic retention and nuclear import of 5S ribosomal RNA containing RNPs.* EMBO J, 1996. **15**(6): p. 1383-91.

39. Chou, H.C., et al., *Hepatitis delta antigen mediates the nuclear import of hepatitis delta virus RNA.* J Virol, 1998. **72**(5): p. 3684-90.

40. Gao, R., P. Liu, and S.M. Wong, *Identification of a plant viral RNA genome in the nucleus.* PLoS One, 2012. **7**(11): p. e48736.

41. Kramer, E.B. and A.K. Hopper, *Retrograde transfer RNA nuclear import provides a new level of tRNA quality control in Saccharomyces cerevisiae.* Proc Natl Acad Sci U S A, 2013. **110**(52): p. 21042-7.

42. Chaturvedi, S., K. Kalantidis, and A.L. Rao, *A bromodomain-containing host protein mediates the nuclear importation of a satellite RNA of Cucumber mosaic virus.* J Virol, 2014. **88**(4): p. 1890-6.

43. Ma, J., et al., *A nuclear import pathway exploited by pathogenic noncoding RNAs.* Plant Cell, 2022.

44. Gozmanova, M., et al., *Characterization of the RNA motif responsible for the specific interaction of potato spindle tuber viroid RNA (PSTVd) and the tomato protein Virp1.* Nucleic Acids Res, 2003. **31**(19): p. 5534-43.

45. Maniataki, E., et al., *Viroid RNA systemic spread may depend on the interaction of a 71-nucleotide bulged hairpin with the host protein VirP1.* Rna, 2003. **9**(3): p. 346-54.

46. Torres-Larios, A., et al., *Structural basis of translational control by Escherichia coli threonyl tRNA synthetase.* Nat Struct Biol, 2002. **9**(5): p. 343-7.

47. Lescoute, A., et al., *Recurrent structural RNA motifs, Isostericity Matrices and sequence alignments.* Nucleic Acids Res, 2005. **33**(8): p. 2395-409.

48. Iacoangeli, A. and H. Tiedge, *Translational control at the synapse: role of RNA regulators.* Trends Biochem Sci, 2013. **38**(1): p. 47-55.

49. Drsata, T., et al., *rRNA C-Loops: Mechanical Properties of a Recurrent Structural Motif.* J Chem Theory Comput, 2017. **13**(7): p. 3359-3371.

50. Johnson, P.Z., et al., *RNA2Drawer: geometrically strict drawing of nucleic acid structures with graphical structure editing and highlighting of complementary subsequences.* RNA Biol, 2019. **16**(12): p. 1667-1671.

51. Cocozaki, A.I., et al., *Resistance mutations generate divergent antibiotic susceptibility profiles against translation inhibitors.* Proc Natl Acad Sci U S A, 2016. **113**(29): p. 8188-93.

52. Klein, D., P. Moore, and T. Steitz, *The roles of ribosomal proteins in the structure assembly, and evolution of the large ribosomal subunit.* Journal of molecular biology, 2004. **340**(1): p. 141-177.

53. Zhang, J., et al., *Molecular mechanisms for the regulation of histone mRNA stem-loop-binding protein by phosphorylation.* Proc Natl Acad Sci U S A, 2014. **111**(29): p. E2937-46.

54. Borovinskaya, M.A., et al., *Structural basis for aminoglycoside inhibition of bacterial ribosome recycling.* Nat Struct Mol Biol, 2007. **14**(8): p. 727-32.

55. Ding, B., et al., *Cell-to-cell movement of potato spindle tuber viroid.* Plant J, 1997. **12**(4): p. 931-6.

56. Qi, Y., et al., *Direct role of a viroid RNA motif in mediating directional RNA trafficking across a specific cellular boundary.* Plant Cell, 2004. **16**(7): p. 1741-52.

57. Wassenegger, M., et al., *A single nucleotide substitution converts potato spindle tuber viroid (PSTVd) from a noninfectious to an infectious RNA for nicotiana tabacum.* Virology, 1996. **226**(2): p. 191-7.

58. Zhong, X., et al., *Tertiary structure and function of an RNA motif required for plant vascular entry to initiate systemic trafficking.* EMBO J, 2007. **26**(16): p. 3836-46.

59. Vargason, J.M., et al., *Size selective recognition of siRNA by an RNA silencing suppressor.* Cell, 2003. **115**(7): p. 799-811.

60. Klein, D.J., P.B. Moore, and T.A. Steitz, *The roles of ribosomal proteins in the structure assembly, and evolution of the large ribosomal subunit.* J Mol Biol, 2004. **340**(1): p. 141-77.

61. Zhong, X., et al., *A genomic map of viroid RNA motifs critical for replication and systemic trafficking.* Plant Cell, 2008. **20**(1): p. 35-47.

62. Wu, J., et al., *A three-dimensional RNA motif mediates directional trafficking of Potato spindle tuber viroid from epidermal to palisade mesophyll cells in Nicotiana benthamiana.* PLoS Pathog, 2019. **15**(10): p. e1008147.

63. Zirbel, C.L., et al., *Identifying novel sequence variants of RNA 3D motifs.* Nucleic Acids Res, 2015. **43**(15): p. 7504-20.

64. Zanier, K., et al., *Structure of the histone mRNA hairpin required for cell cycle regulation of histone gene expression.* RNA, 2002. **8**(1): p. 29-46.

65. Takeda, R., et al., *A three-dimensional RNA motif in Potato spindle tuber viroid mediates trafficking from palisade mesophyll to spongy mesophyll in Nicotiana benthamiana.* Plant Cell, 2011. **23**(1): p. 258-72.

66. Jiang, D., M. Wang, and S. Li, *Functional analysis of a viroid RNA motif mediating cell-to-cell movement in Nicotiana benthamiana.* J Gen Virol, 2017. **98**(1): p. 121-125.

67. Takeda, R., et al., *Allelic RNA Motifs in Regulating Systemic Trafficking of Potato Spindle Tuber Viroid.* Viruses, 2018. **10**(4).

68. Brioudes, F., et al., *HASTY, the Arabidopsis EXPORTIN5 ortholog, regulates cell-to-cell and vascular microRNA movement.* EMBO J, 2021. **40**(15): p. e107455.

69. Haywood, V., F. Kragler, and W.J. Lucas, *Plasmodesmata: pathways for protein and ribonucleoprotein signaling.* Plant Cell, 2002. **14 Suppl**: p. S303-25.

70. Levy, A., et al., *A plasmodesmata-associated beta-1,3-glucanase in Arabidopsis.* Plant J, 2007. **49**(4): p. 669-82.

71. Brunkard, J.O., A.M. Runkel, and P.C. Zambryski, *The cytosol must flow: intercellular transport through plasmodesmata.* Curr Opin Cell Biol, 2015. **35**: p. 13-20.

72. Lee, J.Y., *Plasmodesmata: a signaling hub at the cellular boundary.* Curr Opin Plant Biol, 2015. **27**: p. 133-40.

73. Stephenson, J.D., et al., *Characterizing 3D RNA structure by single molecule FRET.* Methods, 2016. **103**: p. 57-67.

74. Yu, A.M. and J.B. Lucks, *Tracking RNA structures as RNAs transit through the cell.* Nat Struct Mol Biol, 2019. **26**(4): p. 256-257.

75. Cawte, A.D., P.J. Unrau, and D.S. Rueda, *Live cell imaging of single RNA molecules with fluorogenic Mango II arrays.* Nat Commun, 2020. **11**(1): p. 1283.

76. Schmidt, A., et al., *Following the messenger: Recent innovations in live cell single molecule fluorescence imaging.* Wiley Interdiscip Rev RNA, 2020. **11**(4): p. e1587.

77. Zhang, W., et al., *tRNA-Related Sequences Trigger Systemic mRNA Transport in Plants.* Plant Cell, 2016. **28**(6): p. 1237-49.

78. Branch, A.D., B.J. Benenfeld, and H.D. Robertson, *Ultraviolet light-induced crosslinking reveals a unique region of local tertiary structure in potato spindle tuber viroid and HeLa 5S RNA.* Proc Natl Acad Sci U S A, 1985. **82**(19): p. 6590-4.

79. Szymanski, M., et al., *5 S rRNA: structure and interactions.* Biochem J, 2003. **371**(Pt 3): p. 641-51.

80. Wang, Y., et al., *A Land Plant-Specific Transcription Factor Directly Enhances Transcription of a Pathogenic Noncoding RNA Template by DNA-Dependent RNA Polymerase II.* Plant Cell, 2016. **28**(5): p. 1094-107.

81. Gosai, S.J., et al., *Global analysis of the RNA-protein interaction and RNA secondary structure landscapes of the Arabidopsis nucleus.* Mol Cell, 2015. **57**(2): p. 376-88.

82. Tack, D.C., et al., *Tissue-specific changes in the RNA structurome mediate salinity response in Arabidopsis.* RNA, 2020. **26**(4): p. 492-511.

83. Liu, Z., et al., *In vivo nuclear RNA structurome reveals RNA-structure regulation of mRNA processing in plants.* Genome Biol, 2021. **22**(1): p. 11.

84. Song, J., et al., *Transcriptome-Wide Annotation of m(5)C RNA Modifications Using Machine Learning.* Front Plant Sci, 2018. **9**: p. 519.

85. Tang, Y., et al., *OsNSUN2-Mediated 5-Methylcytosine mRNA Modification Enhances Rice Adaptation to High Temperature.* Dev Cell, 2020. **53**(3): p. 272-286 e7.

86. Di Serio, F., et al., *Reassessment of Viroid RNA Cytosine Methylation Status at the Single Nucleotide Level.* Viruses, 2019. **11**(4).

87. Jones, J.D. and J.L. Dangl, *The plant immune system.* Nature, 2006. **444**(7117): p. 323-9.

88. Wang, Y., *Current view and perspectives in viroid replication.* Curr Opin Virol, 2021. **47**: p. 32-37.

89. Jiang, J., et al., *Combining a Simple Method for DNA/RNA/Protein Co-Purification and Arabidopsis Protoplast Assay to Facilitate Viroid Research.* Viruses, 2019. **11**(4).

90. Ding, S.W., *RNA-based antiviral immunity.* Nat Rev Immunol, 2010. **10**(9): p. 632-44.

91. Dadami, E., et al., *DICER-LIKE 4 but not DICER-LIKE 2 may have a positive effect on potato spindle tuber viroid accumulation in Nicotiana benthamiana.* Mol Plant, 2013. **6**(1): p. 232-4.

92. Katsarou, K., et al., *Combined Activity of DCL2 and DCL3 Is Crucial in the Defense against Potato Spindle Tuber Viroid.* PLOS Pathogens, 2016. **12**(10): p. e1005936.

93. Itaya, A., et al., *A structured viroid RNA serves as a substrate for dicer-like cleavage to produce biologically active small RNAs but is resistant to RNA-induced silencing complex-mediated degradation.* J Virol, 2007. **81**(6): p. 2980-94.

94. Minoia, S., et al., *Specific argonautes selectively bind small RNAs derived from potato spindle tuber viroid and attenuate viroid accumulation in vivo.* J Virol, 2014. **88**(20): p. 11933-45.

95. Wassenegger, M. and G. Krczal, *Nomenclature and functions of RNA-directed RNA polymerases.* Trends Plant Sci, 2006. **11**(3): p. 142-51.

96. Hamilton, A., et al., *Two classes of short interfering RNA in RNA silencing.* Embo j, 2002. **21**(17): p. 4671-9.

97. Qu, F., X. Ye, and T.J. Morris, *Arabidopsis DRB4, AGO1, AGO7, and RDR6 participate in a DCL4-initiated antiviral RNA silencing pathway negatively regulated by DCL1.* Proc Natl Acad Sci U S A, 2008. **105**(38): p. 14732-7.

98. Xie, Z., et al., *DICER-LIKE 4 functions in trans-acting small interfering RNA biogenesis and vegetative phase change in Arabidopsis thaliana.* Proc Natl Acad Sci U S A, 2005. **102**(36): p. 12984-9.

99. Naoi, T., et al., *Suppression of RNA-dependent RNA polymerase 6 in tomatoes allows potato spindle tuber viroid to invade basal part but not apical part including pluripotent stem cells of shoot apical meristem.* PLOS ONE, 2020. **15**(7): p. e0236481.

100. Di Serio, F., et al., *RNA-dependent RNA polymerase 6 delays accumulation and precludes meristem invasion of a viroid that replicates in the nucleus.* J Virol, 2010. **84**(5): p. 2477-89.

101. Zheng, Y., et al., *Comprehensive transcriptome analyses reveal that potato spindle tuber viroid triggers genome-wide changes in alternative splicing, inducible trans-acting activity of phased secondary small interfering RNAs, and immune responses.* Journal of Virology, 2017. **91**(11): p. e00247-17.

102. Fei, Q., R. Xia, and B.C. Meyers, *Phased, secondary, small interfering RNAs in posttranscriptional regulatory networks.* Plant Cell, 2013. **25**(7): p. 2400-15.

103. Xie, Z., et al., *Genetic and functional diversification of small RNA pathways in plants.* PLoS Biol, 2004. **2**(5): p. E104.

104. Brosseau, C., et al., *Natural variation in the Arabidopsis AGO2 gene is associated with susceptibility to potato virus X.* New Phytol, 2020. **226**(3): p. 866-878.

105. Qi, Y., et al., *Direct role of a viroid RNA motif in mediating directional RNA trafficking across a specific cellular boundary.* Plant Cell, 2004. **16**(7): p. 1741-52.

106. Flores, R., et al., *Viroid pathogenesis: A critical appraisal of the role of RNA silencing in triggering the initial molecular lesion.* FEMS Microbiology Reviews, 2020. **44**(3): p. 386-398.

107. Navarro, B., R. Flores, and F. Di Serio, *Advances in viroid-host interactions.* Annu. Rev. Virol, 2021. **8**(1): p. 305-325.

108. Gómez, G., G. Martinez, and V. Pallás, *Viroid-induced symptoms in Nicotiana benthamiana plants are dependent on RDR6 activity.* Plant Physiology, 2008. **148**(1): p. 414-423.

109. Li, S., et al., *RNA‐dependent RNA polymerase 1 delays the accumulation of viroids in infected plants.* Molecular Plant Pathology, 2021. **22**(10): p. 1195-1208.

110. Olivier, T. and C. Bragard, *Innate immunity activation and RNAi interplay in citrus exocortis viroid—Tomato pathosystem.* Viruses, 2018. **10**(11): p. 587.

111. Zheng, Y., et al., *Comprehensive transcriptome analyses reveal tomato plant responses to tobacco rattle virus-based gene silencing vectors.* Scientific Reports, 2017. **7**(1): p. 9771.

112. Merkle, T., *Nucleo-cytoplasmic transport of proteins and RNA in plants.* Plant Cell Rep, 2011. **30**(2): p. 153-76.

113. Xu, X.M., et al., *RanGAP1 is a continuous marker of the Arabidopsis cell division plane.* Proceedings of the National Academy of Sciences, 2008. **105**(47): p. 18637-18642.

114. Meier, I. and J. Brkljacic, *The nuclear pore and plant development.* Current Opinion in Plant Biology, 2009. **12**(1): p. 87-95.

115. Frey, S., R.P. Richter, and D. Görlich, *FG-rich repeats of nuclear pore proteins form a three-dimensional meshwork with hydrogel-like properties.* Science, 2006. **314**(5800): p. 815-7.

116. Frey, S. and D. Görlich, *FG/FxFG as well as GLFG repeats form a selective permeability barrier with self-healing properties.* The EMBO Journal, 2009. **28**(17): p. 2554-2567.

117. Stewart, C.L., K.J. Roux, and B. Burke, *Blurring the boundary: the nuclear envelope extends its reach.* Science, 2007. **318**(5855): p. 1408-1412.

118. Chen, C., et al., *Nuclear import of LIKE HETEROCHROMATIN PROTEIN1 is redundantly mediated by importins α-1, α-2 and α-3.* Plant J, 2020. **103**(3): p. 1205-1214.

119. Sarver, M., et al., *FR3D: finding local and composite recurrent structural motifs in RNA 3D structures.* J Math Biol, 2008. **56**(1-2): p. 215-52.

120. Stombaugh, J., et al., *Frequency and isostericity of RNA base pairs.* Nucleic Acids Res, 2009. **37**(7): p. 2294-312.

121. Zhong, X., et al., *Tertiary structural and functional analyses of a viroid RNA motif by isostericity matrix and mutagenesis reveal its essential role in replication.* J Virol, 2006. **80**(17): p. 8566-81.

122. Woo, Y.-M., et al., *Characterization of nuclear import of potato spindle tuber viroid RNA in permeabilized protoplasts.* The Plant Journal, 1999. **17**(6): p. 627-635.

123. Seo, H., K. Kim, and W.J. Park, *Effect of VIRP1 Protein on Nuclear Import of Citrus Exocortis Viroid (CEVd).* Biomolecules, 2021. **11**(1).

124. Rubio, V., et al., *An alternative tandem affinity purification strategy applied to Arabidopsis protein complex isolation.* Plant J, 2005. **41**(5): p. 767-78.

125. Zheng, Y., et al., *Comprehensive transcriptome analyses reveal tomato plant responses to tobacco rattle virus-based gene silencing vectors.* Sci Rep, 2017. **7**(1): p. 9771.

126. Wang, Y., et al., *Evidence for the Existence of the Loop E Motif of Potato Spindle Tuber Viroid In Vivo ▿*. Journal of Virology, 2007. **81**(4): p. 2074-2077.

127. Dissanayaka Mudiyanselage, S.D. and Y. Wang, *Evidence Supporting That RNA Polymerase II Catalyzes De Novo Transcription Using Potato Spindle Tuber Viroid Circular RNA Templates.* Viruses, 2020. **12**(4).

128. Chen, C., et al., *Nuclear import of LIKE HETEROCHROMATIN PROTEIN1 is redundantly mediated by importins alpha-1, alpha-2 and alpha-3.* Plant J, 2020. **103**(3): p. 1205-1214.

129. Yang, X., et al., *Suppression of methylation-mediated transcriptional gene silencing by betaC1-SAHH protein interaction during geminivirus-betasatellite infection.* PLoS Pathog, 2011. **7**(10): p. e1002329.

130. Daròs, J.A. and R. Flores, *Arabidopsis thaliana has the enzymatic machinery for replicating representative viroid species of the family Pospiviroidae.* Proc Natl Acad Sci U S A, 2004. **101**(17): p. 6792-7.

131. Zheng, Y., et al., *Comprehensive Transcriptome Analyses Reveal that Potato Spindle Tuber Viroid Triggers Genome-Wide Changes in Alternative Splicing, Inducible trans-Acting Activity of Phased Secondary Small Interfering RNAs, and Immune Responses.* J Virol, 2017. **91**(11).

132. Martinez de Alba, A.E., et al., *A bromodomain-containing protein from tomato specifically binds potato spindle tuber viroid RNA in vitro and in vivo.* J Virol, 2003. **77**(17): p. 9685-94.

133. Kalantidis, K., et al., *Virp1 is a host protein with a major role in Potato spindle tuber viroid infection in Nicotiana plants.* J Virol, 2007. **81**(23): p. 12872-80.

134. Zuo, J., Q.W. Niu, and N.H. Chua, *Technical advance: An estrogen receptor-based transactivator XVE mediates highly inducible gene expression in transgenic plants.* Plant J, 2000. **24**(2): p. 265-73.

135. Steger, G., *Modelling the three-dimensional structure of the right-terminal domain of pospiviroids.* Sci Rep, 2017. **7**(1): p. 711.

136. Homan, P.J., et al., *Single-molecule correlated chemical probing of RNA.* Proc Natl Acad Sci U S A, 2014. **111**(38): p. 13858-63.

137. Lopez-Carrasco, A. and R. Flores, *Dissecting the secondary structure of the circular RNA of a nuclear viroid in vivo: A "naked" rod-like conformation similar but not identical to that observed in vitro.* RNA Biol, 2017. **14**(8): p. 1046-1054.

138. Zhu, Y., et al., *Movement of potato spindle tuber viroid reveals regulatory points of phloem-mediated RNA traffic.* Plant Physiol, 2002. **130**(1): p. 138-46.

139. Long, J., et al., *Nurse cell–derived small RNAs define paternal epigenetic inheritance in Arabidopsis.* Science, 2021. **373**(6550): p. eabh0556.

140. Afonin, K.A. and N.B. Leontis, *Generating New Specific RNA Interaction Interfaces Using C-Loops.* Journal of the American Chemical Society, 2006. **128**(50): p. 16131-16137.

141. Di Serio, F., et al., *ICTV Virus Taxonomy Profile: Pospiviroidae.* J Gen Virol, 2021. **102**(2).

142. Zuker, M., *Mfold web server for nucleic acid folding and hybridization prediction.* Nucleic Acids Res, 2003. **31**(13): p. 3406-15.

143. Ma, J., S.D.D. Mudiyanselage, and Y. Wang, *Emerging value of the viroid model in molecular biology and beyond.* Virus Research, 2022. **313**: p. 198730.

144. Alba, A.E.M.d., et al., *VIRUS-CELL INTERACTIONS-A Bromodomain-Containing Protein from Tomato Specifically Binds Potato Spindle Tuber Viroid RNA In Vitro and In Vivo.* Journal of Virology, 2003. **77**(17): p. 9685-9694.

145. Gozmanova, M., et al., *Characterization of the RNA motif responsible for the specific interaction of potato spindle tuber viroid RNA (PSTVd) and the tomato protein Virp1.* Nucleic Acids Research, 2003. **31**(19): p. 5534-5543.

146. Takeda, R., et al., *A three-dimensional RNA motif in Potato spindle tuber viroid mediates trafficking from palisade mesophyll to spongy mesophyll in Nicotiana benthamiana.* The Plant Cell, 2011. **23**(1): p. 258-272.

147. Jones, J.D.G. and J.L. Dangl, *The plant immune system.* Nature, 2006. **444**(7117): p. 323-329.

148. Kappagantu, M., et al., *Hop stunt viroid: Effect on Host (Humulus lupulus) Transcriptome and Its Interactions With Hop Powdery Mildew (Podospheara macularis).* Molecular Plant-Microbe Interactions®, 2017. **30**(10): p. 842-851.

149. Hammond, R.W. and Y. Zhao, *Characterization of a tomato protein kinase gene induced by infection by Potato spindle tuber viroid.* Molecular plant-microbe interactions, 2000. **13**(9): p. 903-910.

150. Hammond, R.W. and Y. Zhao, *Modification of tobacco plant development by sense and antisense expression of the tomato viroid-induced AGC VIIIa protein kinase PKV suggests involvement in gibberellin signaling.* BMC Plant Biology, 2009. **9**(1): p. 1-14.

151. Matsushita, Y., H. Yanagisawa, and T. Sano, *Vertical and horizontal transmission of Pospiviroids.* Viruses, 2018. **10**(12): p. 706.

152. Boutrot, F. and C. Zipfel, *Function, discovery, and exploitation of plant pattern recognition receptors for broad-spectrum disease resistance.* Annual review of phytopathology, 2017. **55**: p. 257-286.

153. Erb, M. and P. Reymond, *Molecular interactions between plants and insect herbivores.* Annu. Rev. Plant Biol, 2019. **70**(1): p. 527-557.

154. Hou, S., et al., *Damage-associated molecular pattern-triggered immunity in plants.* Frontiers in plant science, 2019. **10**: p. 646.

155. Fujibayashi, M., T. Suzuki, and T. Sano, *Mechanism underlying potato spindle tuber viroid affecting tomato (Solanum lycopersicum): Loss of control over reactive oxygen species production.* Journal of General Plant Pathology, 2021. **87**(4): p. 226-235.

156. Suzuki, T., et al., *RNAi-mediated down-regulation of Dicer-like 2 and 4 changes the response of 'Moneymaker'tomato to potato spindle tuber viroid infection from tolerance to lethal systemic necrosis, accompanied by up-regulation of miR398, 398a-3p and production of excessive amount of reactive oxygen species.* Viruses, 2019. **11**(4): p. 344.

APPENDIX A

APPENDIX A TABLES

Table A.1 PSTVd progeny in *rdr6* systemic leaves

Strain	**Additional mutations**	**Count**
NB		2
RG1	C230U	1
NT		1
	C117G	1
	C117U	1
Int		3
	G390Δ/G391Δ	1
	U238C	1
	G254C	1
	A182Δ/G314C	1
	C282U	1
	U240A/U309C	1
	A142U/G145Δ/G146Δ/C147Δ/C163U	1

Table A.2 *Arabidopsis* mutant lines

Mutant line	**Gene ID**	**TAIR Accession**
ago2-1	AT1G31280	SALK_003380
dcl2-1	At3G03300	SALK_064627
dcl4-2t	At5G20320	GABI_160G05
dcl2-1/dcl3-1	At3G03300/At3G43920	CS16393
dcl3-1/dcl4-2t	At3G43920/At5G20320	CS66484
rdr2-2	AT4G11130	SALK_059661
rdr6-15	AT3G49500	SAIL_617_H07
sgs3-14	SALK_001393	SALK_001394

Table A.3 Primer sequences

Viroids	**Primer name**	**Sequences**
AFCVd	Oligomer F1	ACGTCTCACATGCGTCGTCGACGAAGGGTCCT
	Oligomer R1	TCGTCTCTAGTCACCAGGTGAGACTTATCCAG
	Oligomer F2	ACGTCTCAGACTCGTCGTCGACGAAGGGTCCT
	Oligomer R2	TCGTCTCTGGCCAGTCACCAGGTGAGACTTATCCAG
ASSVd	Oligomer F1	AGGTCTCACATGCGTCGTCGACGAAGGCCGGT
	Oligomer R1	TGGTCTCTACAGGTGAGTTCCTTCTTCTCCTC
	Oligomer F2	AGGTCTCACTGTCGTCGTCGACGAAGGCCGGT
	Oligomer R2	TGGTCTCTGGCCACAGGTGAGTTCCTTCTTCTCCTC
CBCVd	Oligomer F1	AGGTCTCACATGATCCCCGGGGAAATCTCTTC
	Oligomer R1	TGGTCTCTGGCCTCTTCAGGTATGTTCCCTCC
	Oligomer F2	GATCCCCGGGGAAATCTCTTCAGAC
	Oligomer R2	ACCCGGGGATCCCTCTTCAGGTATGTTCCCTCC
HLVd	Oligomer F1	AGGTCTCACATGATCCCTGGGGAAACCTACTC
	Oligomer R1	TGGTCTCTCCTCTTCGAGCCCTTGCCAC
	Oligomer F2	AGGTCTCAGAGGGATCCCTGGGGAAACCTACTC

Table A.3 (Continued)

Viroids	**Primer name**	**Sequences**
	Oligomer R2	TGGTCTCTGGCCTCTTCGAGCCCTTGCCAC
HSVd	T3-HSVd-f	GGGGACAAGTTTGTACAAAAAAGCAGAATTAACCCTCACTAAAGGCAACTCTTCTCAGA
	RZ-r	CGGGTACCAGGTAATATACCACAAC
	HSVd-f	GCAACTCTTCTCAGAATCCAGCG
	HSVd-r	CCCGGGGCTCCTTTCTCAG
ASBVd	ASBVd-f	TGATCACTTCGTCTCTTCAGGGAAAGA
	ASBVd-r	TGATCAAGAGATTGAAGACGAGTGAACTAATTTTT
PSTVd	95f	GGGGAAACCTGGAGCGAACTGG
	94r	CCCGGGGATCCCTGAAGCGCTCC
*ago*2-1	F	GAGCCGCCAAGGAAGACGTCCA
	R	GAGCCGCCAAGGAAGACGTCCA
*dcl*2-1	F	GCGGAGGCAGGTCTCCTAACTT
	R	GATGTTAACCTACGAATACGAACAGGT
dcl3-1	F	TTGATGCTTCTCTTAGAAGGCTTCAAGAG
	R	CTTGCGGCAAATACACCCCAATGG

Table A.3 (Continued)

Viroids	**Primer name**	**Sequences**
*dcl*4-2t	F	GCTCATGAGAACATAACAACCTCCCA
	R	ATTTCAGGTGGCCTGGTCCTTCC
*rdr*2-2	F	GAGCATGTCTCGGATTTCATGAGAG
	R	GCAGAAGGGACATGACTCAATCC
*rdr*6-15	F	ATGGGGTCAGAGGGAAATATGAAGAAG
	R	CCCAATCTCAAGTGTAATACCAGCCA
*sgs*3-14	F	CGCCTCACCGCATGCATTCTGTGC
	R	CCAGATACGTTGCTACCTCTCCC
	LBa1	TGGTTCACGTAGTGGGCCATCG
	LB1	GCCTTTTCAGAAATGGATAAATAGCCTTGCTTCC
	LB3	TAGCATCTGAATTTCATAACCAATCTCGATACAC

Table A.4 IMPa homologs in tomato

	Arabidopsis	Tomato	**Mock vs PSTVd**									
			Mock_rep1	**Mock_rep2**	**Mock_rep3**	**mean**	**PSTVd_rep1**	**PSTVd_rep2**	**PSTVd_rep3**	**mean**	**ratio**	**adjust p**
IMPa1	*AT3G06720*	*Solyc08g041890.4.1*	44.44426	34.81007	37.2542	38.83618	55.5543	52.47995	40.3205	49.45158	1.273338	0.579912
IMPa2	*AT4G16143*	*Solyc01g060470.3.1*	52.50191	42.06861	44.36111	46.31054	53.5011	83.1585	61.37974	66.01311	1.425445	0.571668
IMPa3	*AT4G02150*	*Solyc06g009750.4.1*	24.4624	13.1345	31.5859	23.06093	23.6453	35.2173	33.6517	30.8381	1.337244	0.569285
IMPa4	*AT1G09270*	*Solyc01g100720.3.1*	64.2503	54.2701	61.9589	60.15977	60.9311	86.568	89.957	79.15203	1.315697	0.384875
IMPa5	*AT5G49310*	NA										
IMPa6	*AT1G02690*	NA										
IMPa7	*AT3G05720*	NA										
IMPa8	*AT5G52000*	NA										
IMPa9	*AT5G03070*	*Solyc10g084270.2.1*	34.196	31.9133	29.4405	31.84993	27.2841	24.5347	11.8683	21.22903	0.666533	0.597647

Table A.4 (Continued)

	Arabidopsis	Tomato	Mock vs TRV									
			Mock_rep1	**Mock_rep2**	**Mock_rep3**	**mean**	**TRV_rep1**	**TRV_rep2**	**TRV_rep3**	**mean**	**ratio**	**adjust p**
IMPa1	*AT3G06720*	*Solyc08g041890.4.1*	44.44426	34.81007	37.2542	38.83618	26.51621	51.2733	41.6038	39.79777	1.02476	0.64774
IMPa2	*AT4G16143*	*Solyc01g060470.3.1*	52.50191	42.06861	44.36111	46.31054	48.6375	41.77939	53.76861	48.06183	1.037816	0.859597
IMPa3	*AT4G02150*	*Solyc06g009750.4.1*	24.4624	13.1345	31.5859	23.06093	12.1259	17.4502	28.3789	19.31833	0.837708	0.927224
IMPa4	*AT1G09270*	*Solyc01g100720.3.1*	64.2503	54.2701	61.9589	60.15977	54.637	66.756	53.7519	58.38163	0.970443	0.786132
IMPa5	*AT5G49310*	NA										
IMPa6	*AT1G02690*	NA										
IMPa7	*AT3G05720*	NA										
IMPa8	*AT5G52000*	NA										
IMPa9	*AT5G03070*	*Solyc10g084270.2.1*	34.196	31.9133	29.4405	31.84993	8.050117	16.95011	13.51699	12.83907	0.403111	0.60616

The normalized reads (FPKM) of tomato IMPas in RNA-Seq dataset are listed. NA, not found.

Table A.5 Primer sequences

	Primer name	**Sequences**
Q-satRNA	f	AGGTCTCACATGTTTTGTTTGTTAGAGAATTGCGTAGAGGGG
	r	TGGTCTCTGGCCGGGTCCTGGTAGGGAATGATAAAC
HSVd	T3-HSVd-f	GGGGACAAGTTTGTACAAAAAAGCAGAATTAACCCTCACTAAAGGCAACTCTTCTCAGA
	RZ-r	CGGGTACCAGGTAATATACCACAAC
	HSVd-f	GCAACTCTTCTCAGAATCCAGCG
	HSVd-r	CCCGGGGCTCCTTTCTCAG
PSTVd	95f	GGGGAAACCTGGAGCGAACTGG
	94r	CCCGGGGATCCCTGAAGCGCTCC
Histone H2A	Nb f	ATGGATACTAGCGGCAAAGCGAAG
	Nb r	CTAAGCCTTCTTAGGAGATTTGGTAG
	RTr	CGAGAACAGCAGCCAAGTAAACG
	Sl f	ATGGAGTCTACCGGAAAAGTGAAG
	Sl r	TGCCTTCTTGGGAGATTTGGTAG
IMPa8	f	ATGGCTTGGAAAACAGAGGTGAACGA
	r	CACCTGAAAGTCCACATCATCACATC
IMPa9	f	ATGGCGGATGATGGCTCCGCCT
	r	TTCATCGATTCCATAATCTTCACCAAAGTATTTATC

Table A.5 (Continued)

	Primer name	**Sequences**
Virp1	f	CACCATGGCTCCGGCTGTTTTCGCTAC
	r	TTAACATTGGGCTTCTTTTGCTTCCAC
LHP1	f	CACCATGAAAGGGGCAAGTGGTGCTG
	r	GGGCGTTCGATTGTACTTGAGATG
Nb *IMPa-4*	BamHI p f	AAGGATCCCTTCGACCCGGCACTCG
	XhoI p r	AAACTCGAGCCTTTTCTCAATAGTGGCAGGT
Sl *IMPa-4*	p f	GCTACCTCTGGAGGATCTAATGA
	p r	GAACATTAGGCTGGTTGTTTCCG
RZ:Int	RZ-f	CACCGGAATTCGAGCTCGGTACCCGG
	RZ-r	CGGGTACCAGGTAATATACCACAAC

Nb, *Nicotiana benthamiana*. Sl, *Solanum lycopersicum* (tomato)

Table A.6 PSTVd and HSVd progeny in systemic leaves

Inoculum	Progeny in systemic leaves	Count
PSTVd U187A	WT	6
	U252A	1
	U24C	1
	U240A	1
	U27C/C102U/C117U/A274G/U356C	1
PSTVd U187C	WT	6
	U187C/A119G	1
	G287A	1
	C117U	1
	A152G	1
HSVd G157C	G157C	5
	G157C/U258C	1
	G157C/A158G/G239A	1